*Geophys. J. Int.* (1993) **115,** 1032–1054 *and Microfiche GJI* 115/1

# Focal mechanisms of large earthquakes in the South Island of New Zealand: implications for the accommodation of Pacific–Australia plate motion

Helen Anderson, Terry Webb and James Jackson*
*Institute of Geological and Nuclear Sciences, PO Box* 1320, *Wellington, New Zealand*

Accepted 1993 May 18. Received 1993 May 17; in original form 1992 October 22

## SUMMARY

The plate motion model NUVEL-1 predicts oblique convergence between the Pacific and Australian plates in the South Island of New Zealand. We used *P* and *SH* body waveform analysis to constrain the focal mechanisms of the 15 largest earthquakes ($M_S > 5.8$) that have occurred in this region since 1964, in order to see how the plate motion is accommodated. At the southern end of the Alpine Fault, convergence is achieved by oblique slip movement along a concentrated zone of deformation. In the southern offshore region one event may be related to thrusting of the Australian plate beneath the Pacific plate, and another strike-slip event probably demonstrates movement on an active strike-slip fault system parallel to, but offset from, the southern limit of the Alpine Fault. This geometry provides a possible mechanism for the rapid uplift of the Fiordland region. Deformation in the northern South Island is more distributed. In the south-west Marlborough region partitioning occurs between strike-slip faulting in the SE and reverse faulting farther NW in the Buller region. We suggest that the partitioning developed as a consequence of an increasing component of shortening that was accommodated by slip on reactivated pre-existing normal faults in the Buller region. Shortening in the Buller region may have deflected the NE end of the Alpine Fault towards the NW, forming the prominent bend. The Marlborough Fault System, with its youngest and most active faults to the SE, probably developed in an attempt to maintain a through-going strike-slip structure as each of the strike-slip faults was transported towards the north-west. Partitioning of the opposite polarity (with reverse faulting SE of the strike-slip faulting) occurs in north-east Marlborough. The boundary between the two different styles of partitioning in NE and SW Marlborough appears to coincide with a change in the nature of the downgoing slab and a change in strike of faults of the Marlborough Fault System. A normal faulting earthquake on the northern edge of the Chatham rise probably results from a complex interaction of the buoyant continental crust in that region with the subduction zone and the overlying Marlborough Fault System.

**Key words:** Alpine fault, earthquakes, Fiordland, focal mechanisms, Marlborough Fault System, seismotectonics.

## INTRODUCTION

In the New Zealand region the deformation between the Pacific and Australian plates is marked by a diffuse band of earthquakes 200–300 km in width (Fig. 1). This is typical of regions where plate boundaries cross continental lithosphere, and is in contrast to the relatively narrow bands of seismicity that mark plate boundary zones in oceanic lithosphere, such as that south of the mainland of New Zealand. Where plate boundaries are narrow zones of deformation, or even single faults, the slip direction on faults in earthquakes is usually close to that of the relative plate motion across the boundary, and such slip vectors

* On leave from: Department of Earth Sciences, Bullard Laboratories, Madingley Road, Cambridge CB3 0EZ, UK.

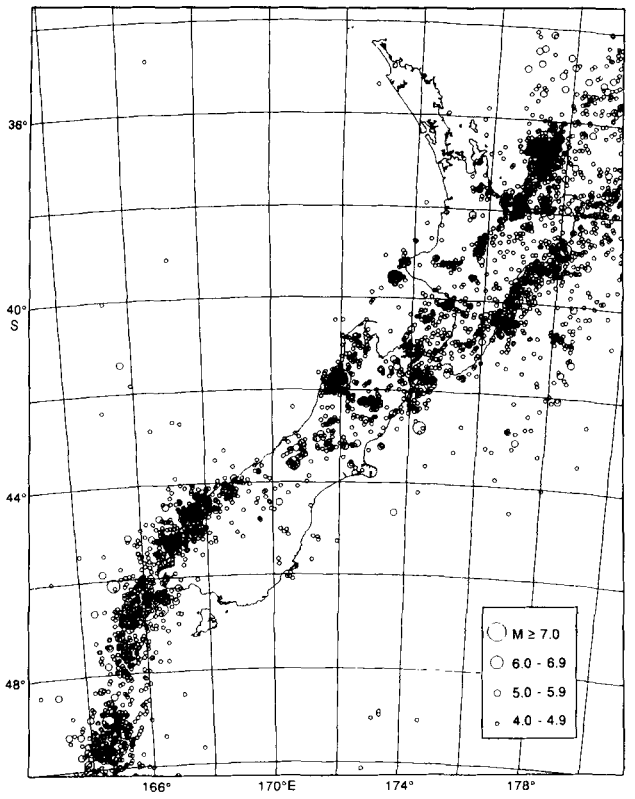


**Figure 1.** Shallow earthquakes (<40 km) of magnitude ≥4.0 reported by the New Zealand Seismological Observatory from 1964 to 1991.

provide constraints on global models of plate motion (e.g. Minster & Jordan 1978; Chase 1978; DeMets *et al.* 1990). As a consequence of the distributed nature of continental deformation, the relationship between the faulting and the overall plate motion is often more complex, as there are a variety of possible ways in which the plate motion may be accommodated. For example, crustal thickening (or thinning), movement of material along the strike of the deforming zone, and rotation of crustal blocks about vertical and horizontal axes are all processes that are known to occur on the continents, sometimes in combination. In any particular deforming continental region two basic questions to address are: (a) how does the present-day deformation of the upper crust accommodate the plate motion, and (b) why it is accommodated in that particular way rather than in any other?

This paper addresses these questions in the South Island of New Zealand, where the convergence between the Pacific and Australian plates occurs at a rate of about 40 mm $yr^{-1}$ in the direction WSW–ENE. Here, as elsewhere, the most obvious and accessible source of information is the orientation of faulting in the largest earthquakes. Earthquakes larger than about $M_S$ 5.8 have rupture dimensions comparable with or larger than the thickness of the upper seismogenic crust. They account for most of the strain that is accommodated by seismic slip on faults (e.g. Molnar 1979; Scholz & Cowie 1990), and often show simpler regional patterns of faulting than the smaller earthquakes that may represent the internal deformation of the blocks bounded by large faults (e.g. Webb & Kanamori 1985; Jones 1988). The motivation of this study was, therefore, to provide the basic data on the focal mechanisms of the larger earthquakes in the South Island, which are essential for an interpretation of the tectonics. The data analysed here include all those available for all the shallow, teleseismically recorded earthquakes since 1964. The data thus form a complete set with which to investigate the large-scale seismic deformation of the South Island during that 28 yr period. In contrast to earlier studies that used only first-motion polarity data to constrain the fault-plane solutions, we use both first-motion and *P*- and *SH*-waveform data, which together provide much better constraints on the focal mechanisms than do first motions alone. Our subsequent interpretation of the tectonics is largely based on these focal mechanisms, though other information, from geodetic or palaeomagnetic measurements (e.g. Bibby 1981; Walcott 1984) is also very important.

The shallow seismicity of the North Island of New Zealand is dominated by the Hikurangi subduction zone and the extensional region above it. The main tectonic element of the South Island is the Alpine Fault (Fig. 2), a dextral strike-slip fault that has had 480 km of displacement since its inception in the Late Oligocene–Early Miocene (Wellman 1953; Berryman *et al.* 1993), with the most recent scarp at its southern onshore limit dated at 230 ± 50 yr BP (Cooper & Norris 1990). In this southern area the surface trace of the Alpine Fault is segmented into short strike-slip and reverse-faulting sections (Norris, Koons & Cooper 1990). In the central South Island the Alpine Fault appears to be a relatively simple feature that is connected to the Hikurangi Subduction zone by the Marlborough Fault System (Fig. 2), which comprises several active dextral strike-slip faults (Lamb & Bibby 1989; Yang 1991). Faults in the south-west Marlborough region such as the Hope Fault (Freund 1971) strike subparallel to the plate-motion direction (DeMets *et al.* 1990). The Alpine Fault forms the western boundary of the Marlborough Fault System and in this region it undergoes a significant bend to the left (Suggate 1979). The Buller region to the west of the bend (Fig. 2) has experienced some major thrust earthquakes on more northerly striking structures in historical times unlike the strike-slip faulting on the Marlborough System. The southern end of the Alpine Fault is not well defined, but it is thought to lie just west of the coast in Fiordland. Beneath the Fiordland block there is a well-defined steeply dipping Benioff zone (Smith & Davey 1984) whose offshore continuation to the south is suspected but not proven. We investigate the relationships of all these different tectonic regimes by determining the focal mechanisms of all the large earthquakes in the South Island.

The data upon which this paper is based are the earthquake source parameters in Tables 1 and 2. Focal mechanisms are discussed in their regional context in the main part of the paper and each one is discussed in detail in Appendix A (on microfiche GJI 115/1).

## Method

Focal mechanisms for New Zealand earthquakes are often difficult to determine reliably from *P*-wave first-motion data alone. Events smaller than magnitude 6 are generally too small for their first motions to be unambiguously recorded

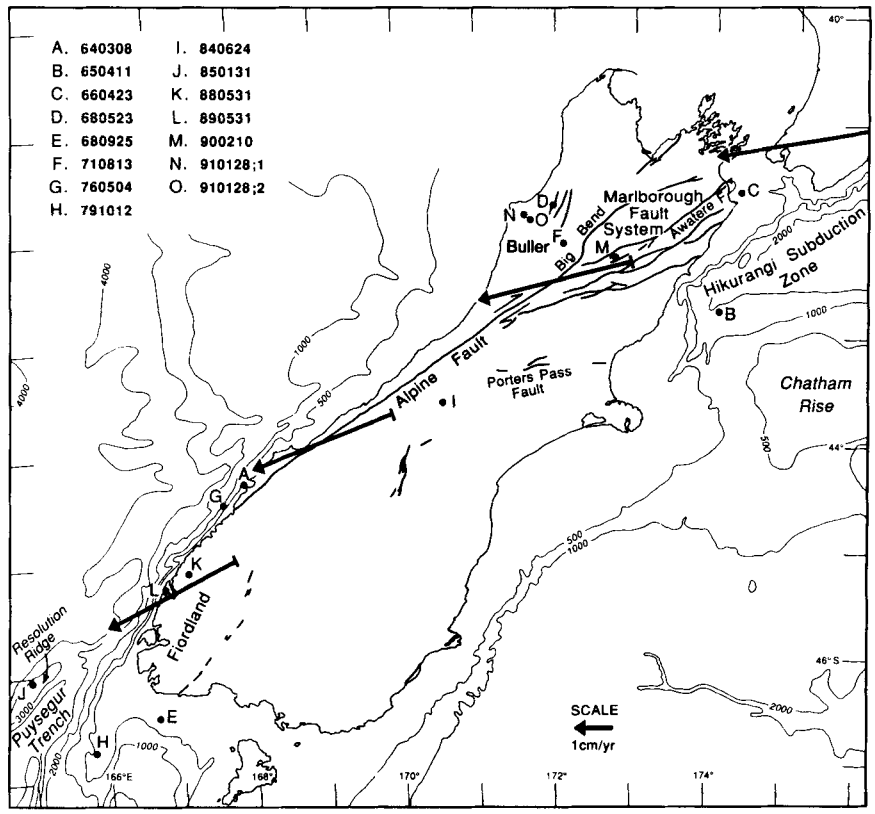


**Figure 2.** The locations of earthquakes considered in this study, numbered according to the key. Quaternary faults are shown as solid lines within the onshore region. Bathymetry contoured in metres. Pacific–Australia relative plate motion (DeMets *et al.* 1990) is shown by a heavy arrow; it is scaled according to the arrow in the lower right.

**Table 1.** Hypocentral parameters for the events in this study.

| Event | date (yrmody) | origin (hrmnsec) | lat. (°) | long. (°) | centroid (km) | $M_S$ | $M_W$ |
|---|---|---|---|---|---|---|---|
| A | 640308 | 013547.5 | -44.30 | 167.87 | 5 | 5.8* | 5.9 |
| B | 650411 | 001110.1 | -42.74 | 174.10 | 16 | 5.8 | 6.1 |
| C | 660423 | 064939.7 | -41.63 | 174.40 | 19 | 5.6* | 5.8 |
| D | 680523 | 172415.6 | -41.76 | 171.96 | 10 | 7.4* | 7.1 |
| E | 680925 | 070248.3 | -46.49 | 166.68 | 4 | 6.2* | 6.3 |
| F | 710813 | 144241.2 | -42.13 | 172.10 | 9 | 5.5* | 5.7 |
| G | 760504 | 135629.1 | -44.67 | 167.45 | 10 | 6.4* | 6.5 |
| H | 791012 | 102519.3 | -46.69 | 165.74 | 12 | 7.2* | 7.3 |
| I | 840624 | 132941.2 | -43.60 | 170.56 | 13 | 6.1* | 6.1 |
| J | 850131 | 043301.1 | -46.06 | 165.03 | 27 | 6.0 | 6.2 |
| K | 880603†† | 232731.6 | -45.10 | 167.17 | 60 | 6.7* | 6.7 |
| L | 890531 | 055422.1 | -45.27 | 166.88 | 24 | 6.2 | 6.4 |
| M | 900210 | 032741.5 | -42.32 | 172.74 | 8 | 6.0† | 5.9 |
| N | 910128 | 125847.6 | -41.89 | 171.58 | 10 | 5.3† | 5.8 |
| O | 910128 | 180053.6 | -41.90 | 171.67 | 12 | 5.6† | 6.0 |

* $M_S$ value from Dowrick & Smith (1990) or Dowrick (1991).
† $M_S$ value from Preliminary Determination of Epicentres, Monthly bulletin, National Earthquake Information Service.
†† Location from Reyners *et al.* (1991).

Note that relocations were performed with depth fixed at the value determined in the minimum misfit solution for each event. Epicentral locations are thought to be accurate to about 10 km; depth uncertainties are listed for each event in Table 2.

All $M_S$ values, except those marked accordingly, are ISC determinations.

**Table 2.** Focal mechanism parameters.

| Date (ymody) | Event | $M_o$ (Nm) | ± | Scale Factor $10^{ex}$ | Strike (°) | ± | Dip (°) | ± | Rake (°) | ± | Depth (km) | ± | Slip Vector (°) | ± | Δ† (sv-calc) |
|---|---|---|---|---|---|---|---|---|---|---|---|---|---|---|---|
| 640308 | A | 7.6 | -*/-3 | 17 | 262 | +10 -5 | 83 | +15 -5 | 147 | +23 -12 | 5 | +15 -5 | 267 | +5 -15 | +20 |
| 650411i | B | 9.4 | +0.3 -4.4 | 17 | 110 | +10 -10 | 55 | +5 -5 | 297 | +13 -37 | 16 | +9 -1 | 158 | +5 -18 | −100 |
| 650411ii | | 5.6 | +0.4 -0.4 | 17 | 103 | +10 -20 | 72 | +18 -8 | 285 | +25 -45 | 16 | +9 -6 | – | – | |
| 660423 | C | 4.6 | +0.7 -0.9 | 17 | 232 | +3 -12 | 68 | +10 -5 | 133 | +10 -10 | 19 | +6 -4 | 254 | +10 -20 | −5 |
| 680523 | D | 4.95 | +0.57 -0.95 | 19 | 232 | +10 -10 | 51 | +7 -7 | 103 | +15 -15 | 10 | +5 -4 | 291 | +9 -11 | +36 |
| 680925i | E | 1.6 | +0.6 -0.6 | 18 | 060 | +10 -10 | 85 | +15 -15 | 182 | +5 -5 | 4 | +16 -4 | 239 | +12 -12 | −3 |
| 680925ii | | 1.2 | – | 18 | 105 | – | 15 | – | 254 | – | 4 | – | | | |
| 710813 | F | 4.0 | +0.5 -0.7 | 17 | 242 | +15 -10 | 83 | +7 -8 | 207 | +15 -12 | 9 | +3 -2 | 238†† | +10 -13 | −17 |
| 760504 | G | 6.5 | +1.5 -1.5 | 18 | 048 | +20 -30 | 47 | +5 -12 | 130 | +10 -20 | 10 | +5 -3 | 268 | +17 -18 | +22 |
| 791012 | H | 7.79 | +3.2 -3.3 | 19 | 007 | +33 -27 | 24 | +5 -5 | 120 | +5 -10 | 12 | +8 -4 | 244 | +10 -5 | +3 |
| 840624 | I | 1.7 | +0.1 -0.2 | 18 | 062 | +5 -12 | 83 | +10 -5 | 206 | +5 -5 | 13 | +2 -3 | 239 | +10 -10 | −13 |
| 850131 | J | 2.0 | +0.3 -0.6 | 18 | 194 | +10 -10 | 57 | +5 -5 | 87 | +10 -8 | 27 | +8 -12 | 290 | +20 -20 | 49 |
| 880603 | K | 1.19 | +0.15 -0.15 | 19 | 281 | +5 -10 | 86 | +5 -7 | 118 | +5 -5 | 60 | +5 -5 | 289 | +15 -5 | ** |
| 890531 | L | 3.45 | +0.35 -0.25 | 18 | 026 | +10 -20 | 48 | +5 -10 | 148 | +7 -10 | 24 | +2 -4 | 229 | +10 -15 | −15 |
| 900210 | M | 8.7 | +0.6 -0.6 | 17 | 055 | +10 -10 | 89 | +5 -5 | 163 | +5 -5 | 8 | +2 -3 | 235 | +10 -7 | −21 |
| 910128a | N | 5.3 | +0.9 -0.7 | 17 | 042 | +20 -10 | 30 | +10 -5 | 99 | +10 -10 | 10 | +3 -2 | 302 | +5 -5 | 47 |
| 910128b | O | 8.7 | +1.7 -0.5 | 17 | 008 | +10 -10 | 48 | +5 -5 | 77 | +10 -5 | 11 | +4 -3 | 297 | +10 -10 | 42 |

* Upper value is not determined because the uncertainty in depth (which is linked to uncertainty in moment) extends to the surface.
** This event was deep and therefore the slip vector is not comparable to the plate-motion direction.
† Observed slip vector minus the plate-motion direction predicted by DeMets *et al.* (1990).
†† If sinistral north-east trending fault is the fault plane, then the slip vector is 330° and Δ = 74°.
Note that the convention adopted for slip-vector orientation is that of the motion of the east or south side relative to the west or north.

by teleseismic stations, in particular island stations whose noise level is often high. First-motion mechanisms of events that are adequately recorded teleseismically are often poorly constrained because the distribution of recording stations is poor, with little or no data in the south-west and south-east azimuthal quadrants (Anderson 1991). Several attempts have been made to complement teleseismic first motions with first motions from regional stations (usually short period, e.g. Davey & Smith 1983) or to produce composite focal mechanisms (e.g. Arabasz & Robinson 1976; Robinson & Arabasz 1975), but since the polarities of New Zealand regional stations have not always been routinely checked, such solutions are often complicated by inconsistent polarities. In this study we use both the first-motion polarities, and teleseismic *P* and *SH* waveforms to constrain the focal mechanisms. The use of *SH* waveforms, which are often larger in amplitude than *P*, allows inclusion of some smaller events ($M_S < 6.0$) and also provides much greater constraint on the orientation of the nodal planes.

In all cases we were able to arrive at a focal mechanism that was consistent with reliable first-motion data and that also produced an acceptable match of observed and synthetic waveforms. An analysis process such as this is now routine and is described in detail by Molnar & Lyon-Caen (1989) and Taymaz, Jackson & Westaway (1990).

## Waveform analysis

We digitized *P* and *SH* waveforms at distances between 30° and 80°, and compared their shapes and amplitudes with synthetic waveforms. To determine the source parameters we used McCaffrey & Abers' (1988) version of Nabelek's (1984) inversion procedure, which minimizes in a weighted least-squares sense the misfit between the recorded and synthetic waveforms (McCaffrey & Nabelek 1987; Nelson, McCaffrey & Molnar 1987; Fredrich, McCaffrey & Denham 1988). Seismograms were generated by combining direct (*P* or *S*) and reflected (*pP* and *sP*, or *sS*) phases from a point source in a given velocity structure. Receiver structure is assumed to be a homogeneous half-space. Amplitudes are adjusted for geometrical spreading, and for attenuation using Futterman's (1962) operator, with $t^* = 1$ s for *P* and $t^* = 4$ s for *SH*. Uncertainties in $t^*$ mainly affect the source duration and seismic moment, rather than the centroid depth or source orientation (Fredrich *et al.* 1988). Seismograms were weighted according to azimuthal density (McCaffrey & Abers 1988) so that stations that were clustered together (in the north-west quadrant in most of our events) had less weight than isolated stations elsewhere (e.g. Pacific Islands and Antarctic). The strike, dip, rake, centroid depth and source-time function, which is described

by a series of overlapping isosceles triangles of prescribed number and duration (Nabelek 1984), are then adjusted in the inversion procedure.

The velocity structure for all the shallow events (<30 km) used a layer over a half-space with the average *P*-wave velocity above the source of 6.0 km s$^{-1}$ and a source *P* velocity of 6.8 km s$^{-1}$. The velocity structure for the only deep event (60 km) used an average crustal velocity above the source of 6.5 km s$^{-1}$, with a mantle-source velocity of 8.1 km s$^{-1}$: a value that is consistent with that determined by Haines (1979). Where the event occurred offshore the appropriate water depth was used, although this was difficult to estimate in regions where bathymetric gradients are steep (e.g. in the Resolution Ridge area, Fig. 2). The effect of steep bathymetric gradients is to produce significant *P*-waveform complexity (Weins 1987, 1989) but this is generally most evident in the later arrivals, and its effect on the inversion is reduced by the inclusion of *SH* waves.

Most of the events were well represented by a single point source, and no event produced a clear azimuthal variation in the waveforms that might indicate rupture propagation. Both these observations are expected from comparison with other studies of similar sized earthquakes (e.g. Taymaz *et al.* 1990; Nelson *et al.* 1987; McCaffrey 1988; Fredrich *et al.* 1988; Molnar & Lyon-Caen 1989).

## Procedure

The details of our analysis procedure will be illustrated with the 1968 May 23 Inangahua earthquake (*D*) (Tables 1 and 2).

We determined the first-motion focal mechanism using teleseismic data, which was then complemented with regional (mostly short period) first motions. The polarities of the short-period regional records are less reliable than the long-period readings. Where polarities from regional stations were necessary to constrain the source mechanism, we calibrated the polarities using a deep distant teleseismic event with an impulsive onset. The first-motion solution was used as a starting model for the waveform inversion procedure. The source orientation of the minimum misfit variance solution returned by the inversion procedure (Fig. 3) was usually consistent with the first-motion data (Fig. 4).

The minimum misfit solution for the Inangahua earthquake (*D*) (Fig. 3) includes a source-time function in which there is a rapid increase in moment release after the first 5 s of rupture. This indicates that the earthquake was a complex event consisting of a small initial subevent ($M_W$ 6.5) followed by a much larger episode of moment release ($M_W$ 7.0). The first two subevents are responsible for the double-upward pulse seen in the onset of the *P* waveforms at all azimuths. The data are not sufficient to resolve either a spatial separation of the subevents or a difference in mechanism between them.

Having found an acceptable minimum misfit solution, we followed the procedure described by McCaffrey & Nabelek (1987), in which the inversion routine is used to carry out tests to determine how well individual source parameters are resolved. We investigated one parameter at a time by fixing it at a series of values either side of the minimum misfit value and then allowing other values in the inversion to vary. We then visually compared the quality of fit between

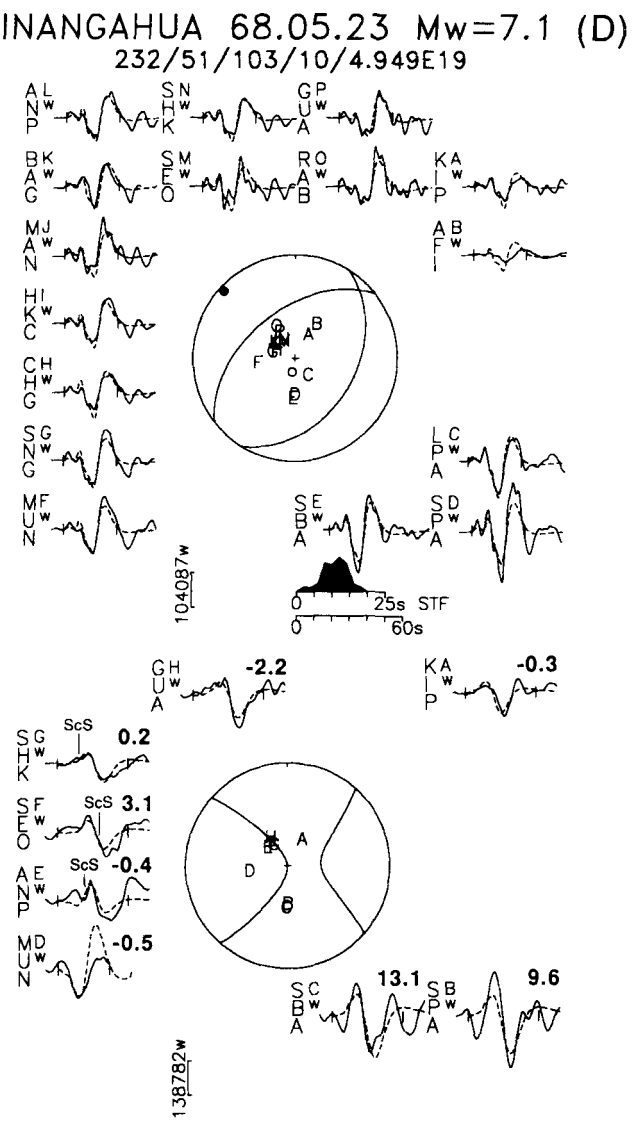


**Figure 3.** This (and subsequent similar figures in Appendix A) shows the radiation patterns and synthetic waveforms for the minimum misfit solution returned by the inversion procedure, as well as the observed waveforms. For the purposes of display, waveform amplitudes have been normalized to that of an instrument with a gain of 3000 at a distance of 40°. Solid lines are observed waveforms, and the inversion window is identified by vertical bars. Synthetic waveforms are dashed lines. The station code is identified to the left of each waveform, together with an upper case letter, which identifies its position on the focal sphere, and a lower case letter that indicates the type of instrument (*w* = WWSSN long period; *d* = GDSN long period). The vertical bar beneath the focal sphere shows the scale in mm, with the lower case letter indicating the instrument type, as before. The source-time function is shown in the middle of the figure, and beneath it is the timescale used for the waveforms. Focal spheres are shown with *P* and *SH* nodal planes, in lower hemisphere projection. Station positions are indicated by letter, and are arranged alphabetically clockwise, starting from north. *P*- and *T*-axes are marked by solid and open circles. Where *ScS* is expected to arrive within the inversion window, its predicted arrival time is marked. Beneath the header at the top of the figure, which shows the date and moment magnitude, are five numbers which show the strike, dip, rake, centroid depth and seismic moment (in units of Nm) of the minimum misfit solution.

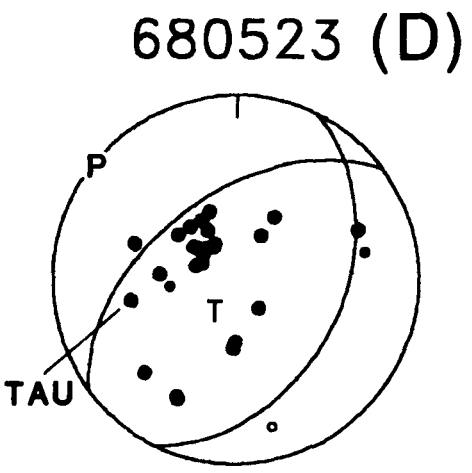


**Figure 4.** Lower hemisphere, equal-area projection of the first-motion polarity data for Inangahua earthquake of 1968 May 23. The dilatational first arrival is indicated by open circles, compressional arrivals are solid. Smaller sized circles and dots indicate short-period, usually regional data. All other polarities were read from long-period vertical WWSSN seismograms. *P*- and *T*-axes are indicated by letter. The date code convention followed in this paper is year, month, day, i.e. 680523 is 1968 May 23.

For the Inangahua earthquake the polarity of the WWSSN station TAU appeared to be anomalous and it is possible to produce a first-motion mechanism that is consistent with TAU. However, this station appears to be anomalous in other events so we were uncertain whether the postion of the station was being determined incorrectly (it is at distances of 10–20°) or there has been a history of polarity reversals. The station log records were checked and in 1968 the station was indeed reversed (June Pongratz, private communication, 1991). The correct polarity plotted in Fig. 4 is consistent with the inversion results.

the observed and synthetic seismograms to determine at what values of the constrained parameters the fit degraded significantly. In this way we were able to estimate the uncertainty in the strike, dip, rake and depth. This procedure was undertaken for all events and the results are listed in Table 2, but only the test results for the Inangahua earthquake are presented here (Figs 5 and 6). The extreme values of strike, dip, rake, slip vector and depth for which the fit is acceptable are shown for comparison with the minimum misfit solution.

Centroid–moment tensor (CMT) solutions (Dziewonski, Chou & Woodhouse 1981) for earthquakes with seismic moment greater than about $10^{17}$ Nm ($M_W \sim 5.3$) are available since 1977. The centroid–moment tensor solutions are usually derived from low-pass filtering the whole wave train at 45 s. The long-period WWSSN data contain higher frequencies, and should be better for constraining the depth and time function. In most cases, the Harvard CMT solution is within the error bounds of our minimum misfit solution. If it is not, we have included in Appendix A (on microfiche GJI 115/1) the waveforms for the CMT solution for comparison with our minimum misfit solution.

Having found the centroid depth, we relocated each event using both teleseismic and regional station data and an appropriate velocity model to determine the origin time, from which we were able to derive residuals for *SH* waves.

The first-motion data, minimum misfit solution and Harvard centroid–moment tensor solution (if available) for all events except the Inangahua earthquake (Fig. 3) are shown in Fig. 7. The location and mechanism data are listed in Tables 1 and 2, and a detailed discussion of each of the other earthquakes, including field data, aftershock studies and previously published focal mechanisms is included in Appendix A (on microfiche GJI 115/1).

## INTERPRETATION

The focal mechanisms and centroid depths for the earthquakes in this study are shown in Fig. 8. The mechanisms for the Solander (E: 1968 September 25), Big Bay (*A*: 1964 March 8) and Chatham Rise (*B*: 1965 April 11) earthquakes are shaded differently in this figure because their minimum misfit solutions are less reliable than the other events in this study. Focal mechanisms derived from surface-faulting observations for the historical Murchison (1929 June 16), Arthurs Pass (1929 March 9) and Glynn Wye (1888 August 31) earthquakes have been included for comparison with the other events in that region. The focal mechanisms for these historic events are discussed in Appendix B (on microfiche GJI 115/1). Slip vectors for the recent events and the plate-motion direction predicted from the Pacific–Australia pole (DeMets *et al.* 1990) are shown in Fig. 9. Identification of a slip vector in each earthquake involves a choice of fault plane from the two nodal planes in each fault-plane solution. Our reasons for making the choices we did are discussed later.

The centroid depths range from 4 to 27 km, with one Fiordland subduction zone event (*K*) at 60 km. It is noticeable that the deepest events (*B, C, L*) are those above the Hikurangi or Fiordland subduction zones, whereas the events in the central and northern South Island have depths of around 10 km. The centroid depth for the Resolution Ridge earthquake (*J*: 1985 January 31) is significantly greater than expected since it occurred in an area of dominantly oceanic crust to the west of the Puysegur trench, which is thought to be the outcrop of a thrust-dipping east (although the seismicity does not show a clearly defined Benioff zone).

The mechanisms fall into five groups; (a) reverse faulting in the Buller region, (b) strike-slip and oblique-slip faulting events associated with the Marlborough Fault System and its offshore extension, (c) oblique-slip events associated with the southern offshore extension of the Alpine Fault and the Puysegur trench, (d) a deep event associated with the Fiordland subduction zone, and (e) a normal-faulting event at the western end of the Chatham Rise.

No large earthquake has been instrumentally recorded on the Alpine Fault *sensu stricto*, although Holocene faulting events with slip components of 7–8 m dextral and up to 1 m vertical have been documented in places from offset stream beds, terraces and other recent features (Beanland 1987). The modern seismicity level of the Alpine Fault is low but our earthquakes show that its extensions into the southern offshore region and into the Marlborough Fault System have been seismically active in the last 30 yr.

### (a) Buller Region reverse-faulting events

The mechanisms of events in group (a) are similar in spite of a large difference in their magnitudes (ranging from $M_W$ 5.8 to $M_W$ 7.1).

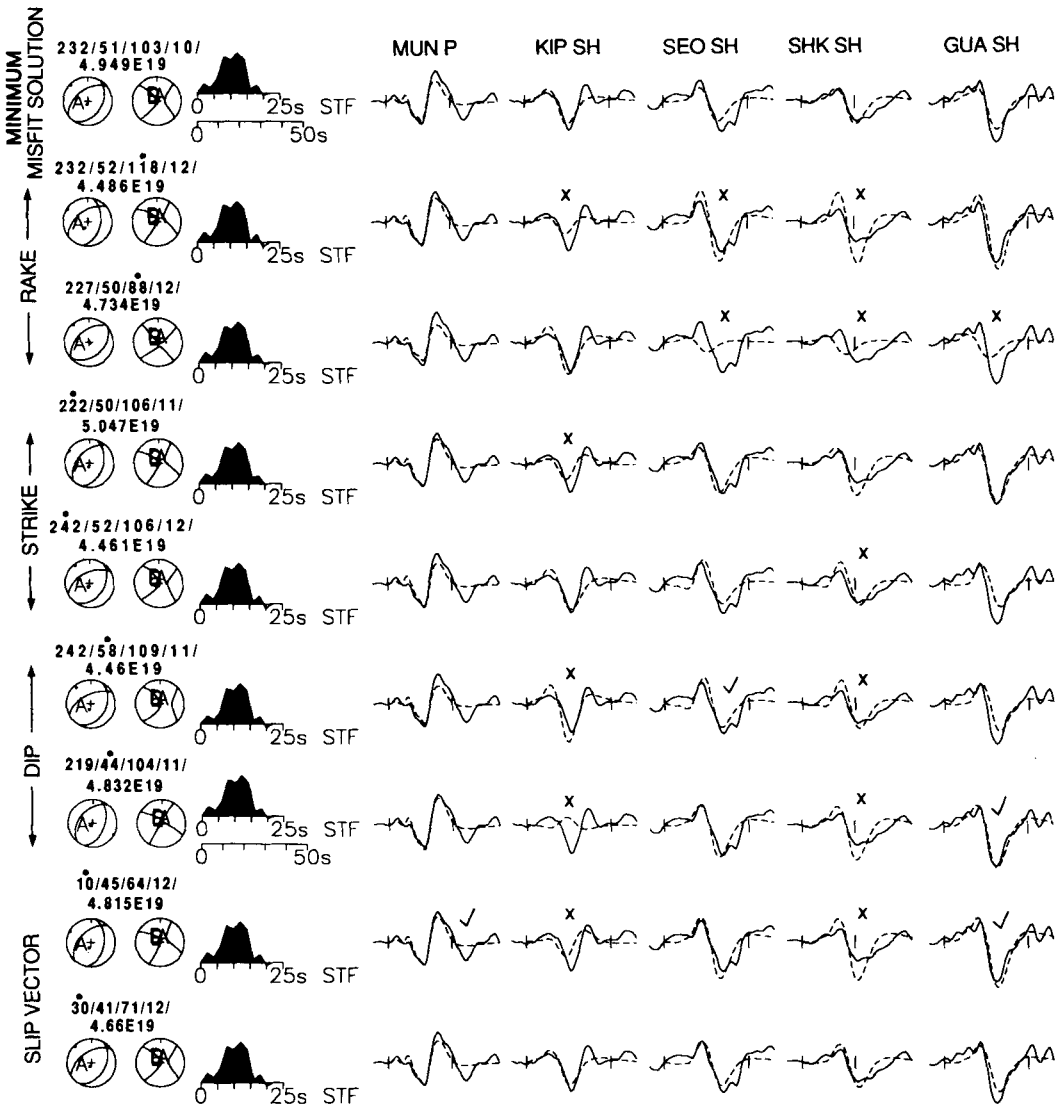


**Figure 5.** In this and Fig. 6, each row shows a selection of waveforms from a run of the inversion program. The top row shows waveforms from the minimum misfit solution. The stations are identified at the top of each column, with the type of waveform marked by *P* or *SH* and followed by the instrument type, as in Fig. 3. At the start of each row are the *P* and *SH* focal spheres for the focal parameters represented by the five numbers (strike, dip, rake, depth and moment, as in Fig. 3) showing the positions on the focal spheres of the stations. A dot above one of the focal parameters means that it was held fixed in that inversion: thus in rows 2–3, 4–5, 6–7 and 8–9 the rake, strike, dip and slip vector were held fixed, respectively. The displayed waveforms are in the same convention as in Fig. 3.

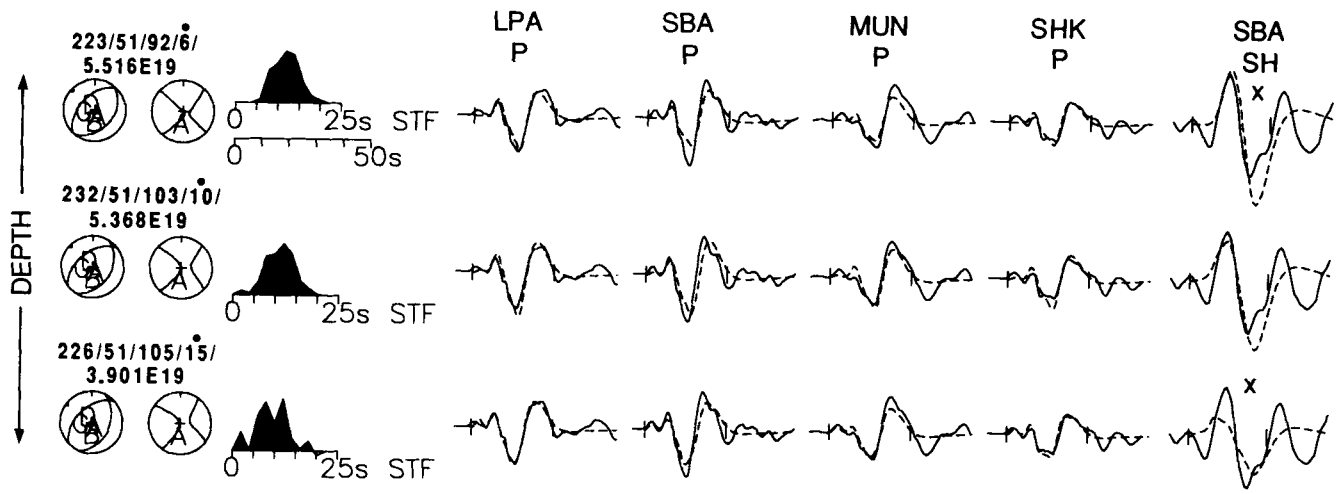


**Figure 6.** As for Fig. 5, except that the range of depths that provide an adequate data fit are shown for comparison.

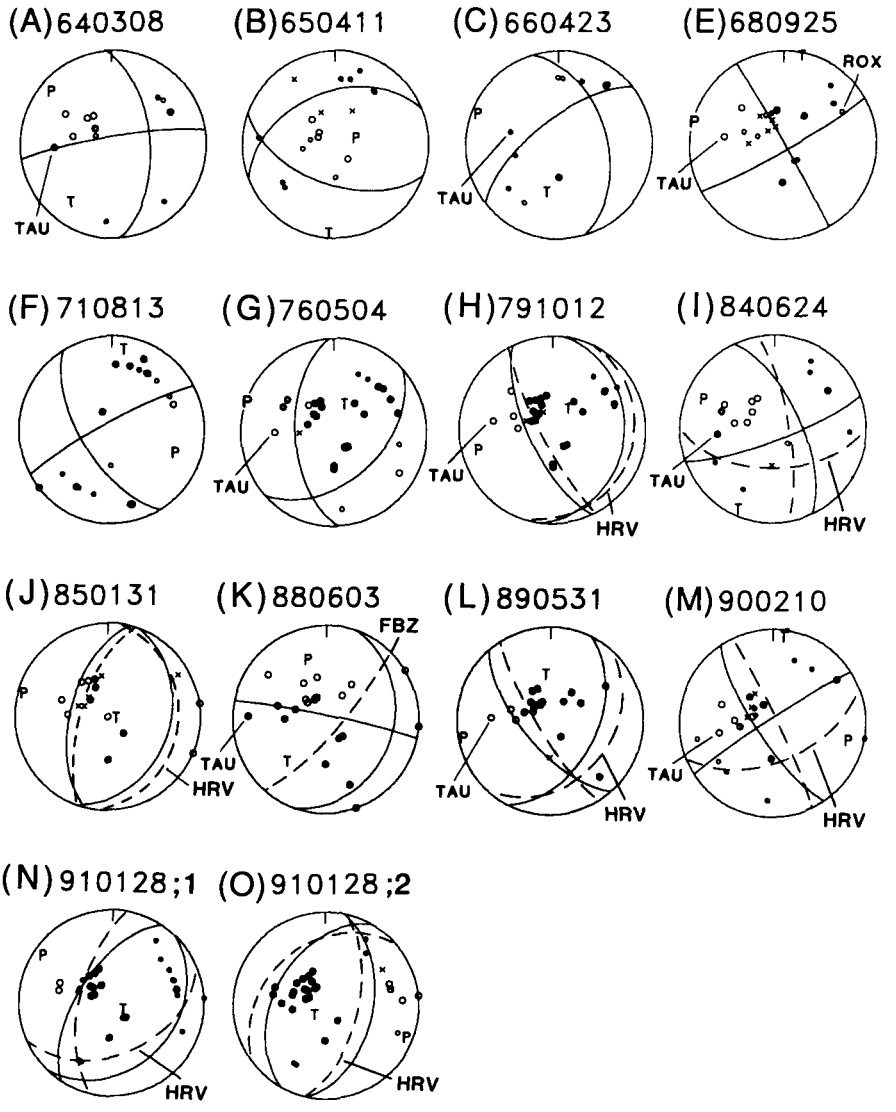


**Figure 7.** Final minimum misfit solutions for each of the earthquakes shown in Fig. 2 except for 1968 May 23 which is shown in Figs 3 and 4. First-motion polarity information is also shown. Dashed nodal planes indicate centroid–moment tensor solution obtained by Harvard University routinely published in *Physics of the Earth and Planetary Interiors*. For several earthquakes the polarity of TAU seems inconsistent. Station records suggest that the polarity of this station was reversed for most of 1968 and possibly late 1979, but station records have not been carefully checked for other time periods. We, therefore, consider TAU to be of unreliable polarity for routine first-motion analysis. It was not used in any waveform inversion because its epicentral distance was <30°. The plane shown as FBZ for *K* indicates the Fiordland Benioff Zone after Smith & Davey (1984).

The largest recent event in the region was the Inangahua earthquake (*D*: 1968 May 23), which had an epicentre located in an area of dense bush and difficult terrain. Although there were several complex ground ruptures, none could be unequivocally identified as the fault break related to the main shock (Lensen & Suggate 1968). The slip vector determined from the focal mechanism cannot, therefore, be directly compared with that from the surface break, but the focal mechanism is consistent with the surface observations of reverse faulting. A sinistral component was reported by Lensen & Suggate (1968) for the most obvious trace, which would be consistent with the south-east-dipping nodal plane being the fault plane. However, recent analysis of repeated levelling surveys in the epicentral area indicates that the fault responsible for uplift in that area dips about 45° to the north-west and probably did not rupture the ground surface (Haines 1991a). Relocated aftershock locations confirm this choice of fault plane (Anderson *et al.* 1994). The slip vector representing movement on the north-west-dipping plane in our minimum misfit solution has an azimuth of 291°, which is 36° clockwise from the plate motion direction predicted by DeMets *et al.* 1990.

In January 1991 two events occurred close together in the region south-west of the Inangahua earthquake. The events (*N* and *O*: Hawks Crag 1 and 2; 1991 January 28) had similar mechanisms to each other and to the Inangahua earthquake. Preliminary aftershock locations (Robinson 1991) for the first Hawks Crag event form a cluster about 8 km to the west of the aftershock sequence for the later earthquake. There is no evidence from the aftershocks or any ground surveys to indicate a preferred fault plane, but because of the dominantly dip-slip character of the

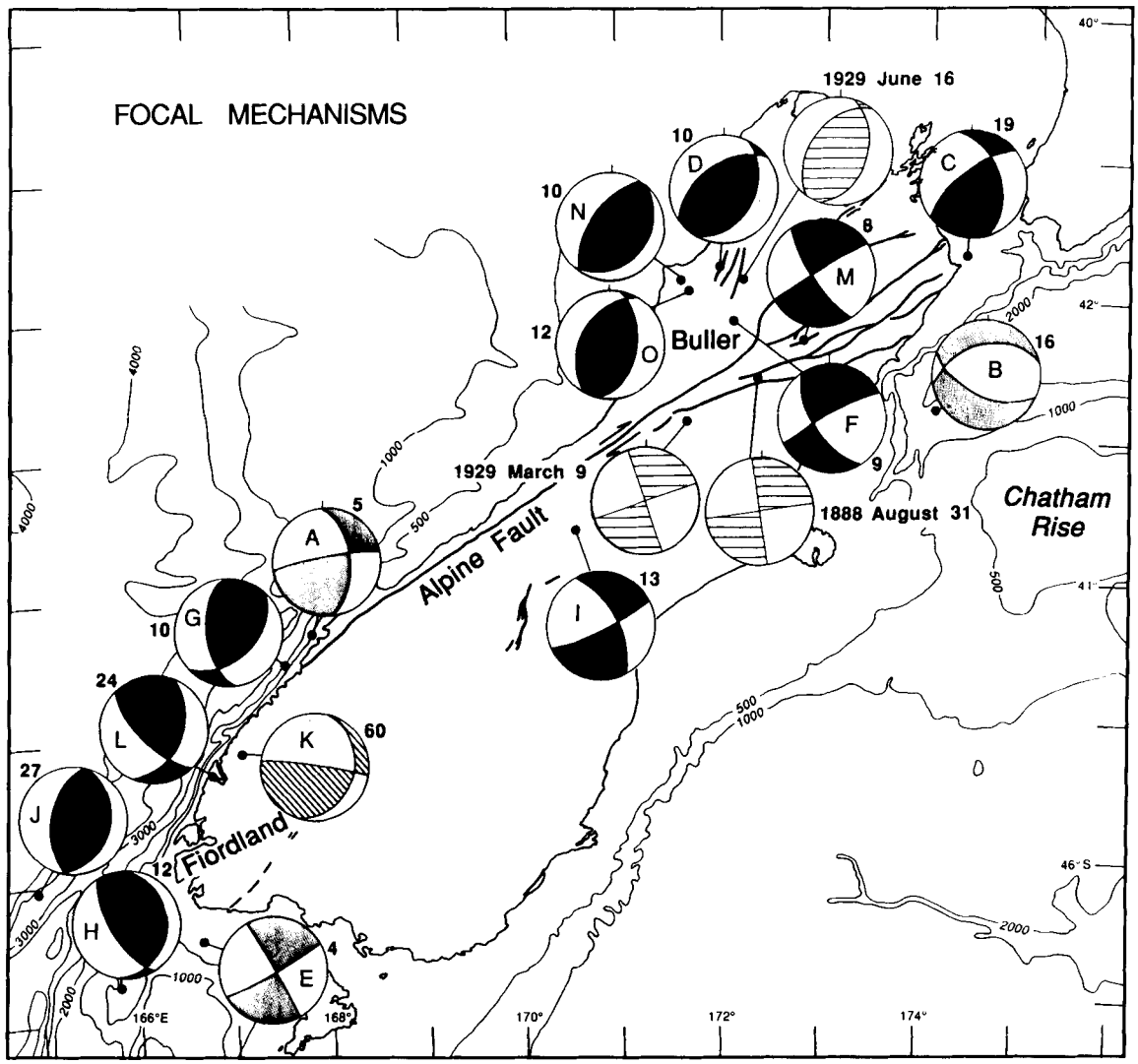


**Figure 8.** Fault-plane solutions for all of the earthquakes in this study and three additional historical events (horizontal lines in compressional quadrants). Criteria for determining historical focal mechanisms are described in Appendix B. The deep Te Anau earthquake has inclined lines and the three least reliable minimum misfit solutions are indicated by grey shading in compressional quadrants. Numbers at the top or side of each focal mechanism indicate the best fit centroid depth.

mechanism, the slip vectors for both nodal planes are very similar.

The Murchison earthquake of 1929 June 16 ($M_S$ 7.8; Dowrick & Smith 1990) also occurred in an area close to the Inangahua event (*D*), and from the surface displacements (see Appendix B on microfiche GJI 115/1), it is possible to determine a focal mechanism, which is similar to those of other events in this region (Fig. 8).

All the large Buller region earthquakes indicate almost pure dip-slip reverse faulting, and their slip vectors are rotated more than 35° clockwise from those predicted by the NUVEL-1 pole (DeMets *et al.* 1990). This discrepancy far exceeds the estimated uncertainties in the slip vectors themselves. These slip vectors are significantly different from those in the Marlborough Fault System to the east.

### (b) Marlborough Fault System

The Tennyson earthquake (*M*: 1990 February 10) occurred in an isolated area between two of the major active faults of the Marlborough Fault System (Fig. 2). No surface rupture was recognized for this event, but preliminary aftershock locations (Webb 1993) are spread over a large area between the Fowlers Fault (Richardson 1977) and the Awatere Fault (Fig. 2). The more precisely located events appear to define an elongate zone, about 12 km long, that is parallel to the local trend of the Awatere Fault, so it is probable that the north-east-striking nodal plane represents the fault plane. The slip vector for this plane is moderately well constrained (235° −7/+10°) and is rotated about 20° anticlockwise relative to the predicted plate-motion direction. Other large strike-slip events have occurred in historical time (150 yr) in the Marlborough region (Cowan 1990; Yang 1992) and surface ruptures have clearly demonstrated dextral motion on the ENE-trending faults (Cowan 1990).

The Maruia Springs earthquake (*F*: 1971 August 13) has a mechanism and slip vector similar to the Tennyson event. Its location west of the Alpine Fault is confirmed by an aftershock study which showed no obvious alignment of aftershocks whose depths ranged between 4 and 14 km

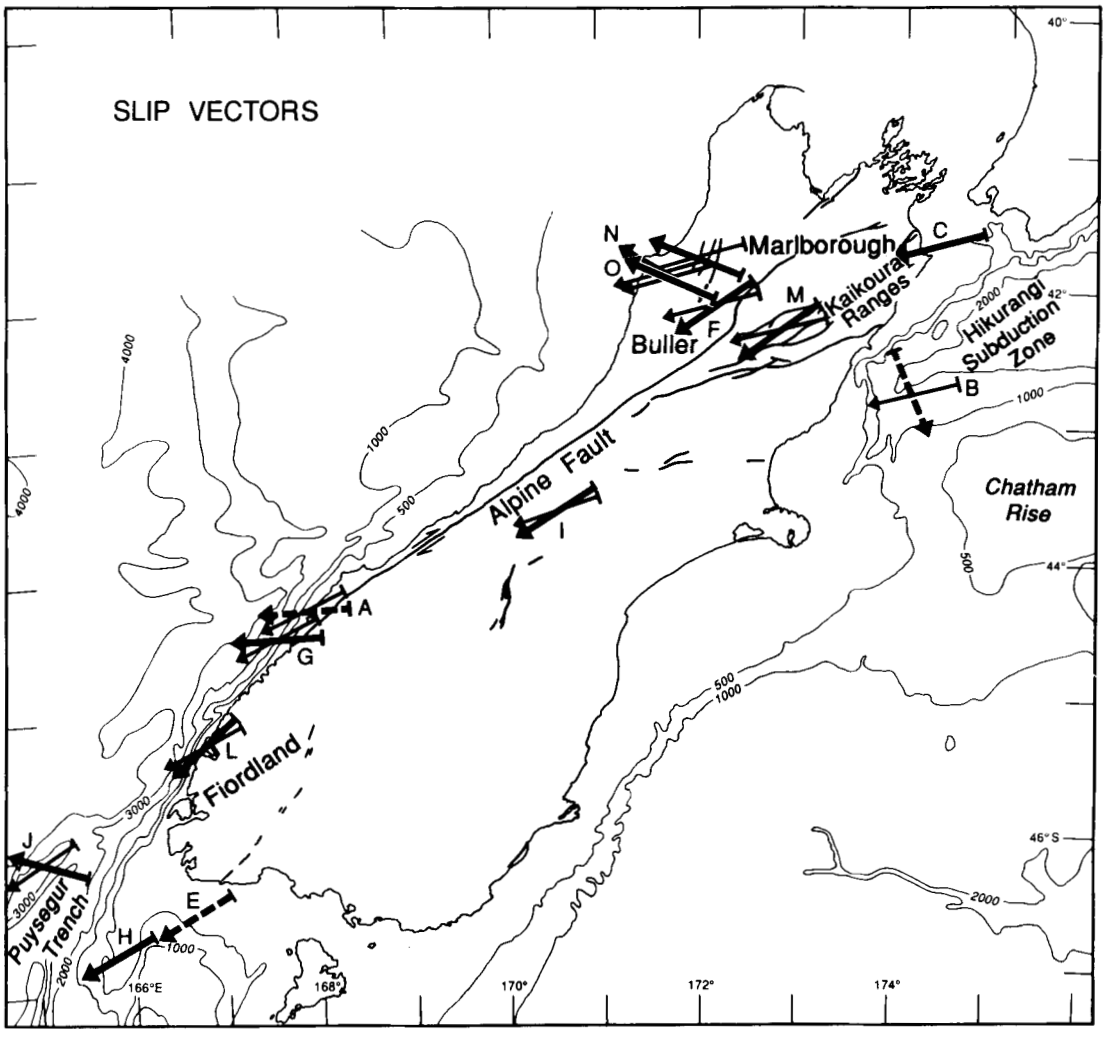


**Figure 9.** Observed slip vector (see Table 2 for errors) for each of the events in this study compared to the predicted plate motion (finer arrow) using the NUVEL-1 pole (DeMets *et al.* 1990). Convention used for defining the slip-vector direction is that the arrow points in the direction of motion of the east or south side relative to the north or west. If no fine arrow is shown, the predicted plate motion and observed slip vector are the same. Dashed slip vectors denote less reliable mechanisms.

(Martin Reyners, private communication). There was no surface rupture identified for this event so the fault plane cannot be unambiguously identified. If the north-west-striking plane were the fault plane, then it would be a sinistral movement with a slip-vector azimuth similar to those of the reverse faulting events in the Buller region. In a more likely interpretation, the north-east-striking plane represents the fault plane, so its strike would be similar to that of the Alpine Fault to the north of the Big Bend (Fig. 2) where there is evidence for minor faults with this trend in the local geology (Cutten 1979).

The Godley River earthquake (*I*: 1984 June 24) occurred in winter in a rugged area of the central Southern Alps, but not on the Alpine Fault. Access to the area in which any ground rupture might be exposed was impossible, although the epicentral area was inspected by air. The fault-plane solution for this event is similar to those in the Marlborough Fault System to the north-east. We consider the the NE striking plane is mostly likely to represent the fault plane and hence that the movement was right-lateral strike slip. No active fault has ben recognized in the epicentral area (Lensen 1977) although if the Porters Pass Fault, which has a similar strike (Berryman 1979) to our preferred fault plane, is projected along strike towards the south-west, then it intersects the epicentral area. We, therefore, suggest that the Godley River earthquake involved motion at the southernmost extent of the Marlborough Fault System.

The Seddon earthquake (*C*: 1966 April 23) occurred at the northern offshore extension of the Marlborough Fault System. It was felt over a large area (Adams 1970), but no surface faulting was identified (Lensen 1970). We consider that the north-east-striking nodal plane is the most likely fault plane because this is the strike of the major faults in this region (Lamb & Bibby 1989, Fig. 2). If so, the movement was oblique, reverse and right-lateral strike slip, with a slip vector virtually the same as that predicted by the plate motions.

All the dominantly strike-slip events (*I, F, M*) have slip vectors that are slightly rotated anticlockwise relative to the plate-motion direction predicted by the NUVEL-1 pole

(DeMets *et al.* 1990). This discrepancy is small (<20°) and is not much greater than the estimated uncertainty in the slip vectors themselves, but is always in the same sense (Table 2).

### (c) Southern Region shallow events

The events in this group split into two separate subsets; oblique-slip events located at the southern end of the Alpine Fault, and a group of dominantly dip-slip or strike-slip events in the extreme south near the Puysegur trench.

The events at the southern end of the Alpine Fault (*A*: Big Bay, 1964 March 8; *G*: Milford Sound, 1976 May 4; *L*: Doubtful Sound, 1989 May 31) have oblique-slip mechanisms with a dominant reverse-faulting component. Choosing the fault plane and hence the slip vector is complicated by the fact that all these events occur offshore or in difficult terrain.

The epicentre for the Big Bay event (*A*) was offshore, but less than 20 km from the Alpine Fault. Neither of the nodal planes in its oblique-slip mechanism has a strike similar to the Alpine Fault, but we have chosen the east-west-striking plane as the most likely fault plane because the motion would be dextral on a fault with this orientation. The slip vector for this fault plane is rotated about 20° clockwise of the predicted plate motion.

The Milford Sound earthquake event (*G*) has a better constrained, dominantly reverse faulting oblique-slip mechanism. It occurred just off the mouth of Milford Sound (Eiby 1978), and aftershocks were also concentrated in this region (Davey & Smith 1983). Identification of the north-east striking plane as the fault plane is based on similarity of strike with the local expression of the Alpine Fault (Fig. 2) and bathymetric trends in the epicentral region. In this case the slip vector is oriented amost east–west and, like event *A*, it is rotated clockwise of the predicted plate motion.

The depth of the Doubtful Sound earthquake (*L*) is significantly greater than the two other shallow Fiordland events (*G* and *A*). This is probably because the two earlier events are to the north of the main Benioff zone (Reyners, Gledhill & Waters 1991, Fig. 2b) and are more closely related to the offshore extension of the Alpine Fault. Like the northern two events in this region, the mechanism involved oblique slip on a reverse fault. We prefer the east-dipping plane as the fault plane because the strike is subparallel to the coast line and bathymetry where it would intersect the surface, and it would involve dextral strike-slip motion in a direction comparable to the predicted plate-motion direction.

The fault plane, and hence the slip vector, cannot be unambiguously identified for any of these focal mechanisms, but dextral movement on north-east-striking planes is most likely, because this is the sense of motion on the Alpine Fault. There appears to be a systematic change in the strike of the north-east striking plane (which we prefer as the fault plane) from almost ~ENE for the Big Bay event through to a more ~NNE strike for the Doubtful Sound event (*L*). The slip vectors of the two most northerly events (*A*, *G*) are rotated about 20° clockwise relative to the plate-motion direction, whereas the Doubtful Sound event is rotated about 15° anticlockwise. However, these discrepancies are comparable with the estimated uncertainties in the slip vectors.

The most southerly group of events includes J: Resolution Ridge, 1985 January 31; *H*: Puysegur, 1979 October 12; and E: Solander, 1968 September 25.

The tectonic significance of the Puysegur earthquake (*H*) lies in the fact that it is the only thrust-faulting earthquake whose epicentre lies east of the Puysegur Trench (Fig. 2). Although it is widely assumed that the Fiordland Benioff zone continues offshore to the south, the seismicity in the offshore region does not clearly define a Benioff zone. If the Puysegur earthquake occurred on a shallow-dipping, north-striking fault then it represents thrusting of oceanic material beneath the continent to the NE. The presence of 2 Myr old andesite volcanic rocks (Reay 1986) at a small island about 100 km east of the epicentre, suggests that subduction has occurred in the region, although the definition of the Benioff zone at depth remains a problem. The slip vector for the shallow-dipping plane has an azimuth indistinguishable from the plate-motion direction.

In spite of its relatively poorly constrained focal mechanism, we are confident that the Solander earthquake (*E*) involved dominantly strike-slip motion (see Appendix A on microfiche GJI 115/1). The epicentre lies on the offshore extension of the Fiordland Boundary Fault Zone (Grant 1985, or Moonlight Fault System of Norris & Carter 1982), which has a similar strike to the north-east-striking plane in our mechanism. Recent movement on this fault zone is demonstrated by offset of the sea-floor (Grant 1985). It seems likely that the north-east-striking plane in the fault-plane solution is, therefore, the fault plane, which moved in a dextral strike-slip sense. The slip vector for this fault plane is the same as the predicted plate-motion direction but is poorly constrained.

Resolution Ridge earthquake (*J*) was a relatively deep event (27 km) with a mechanism that was almost pure dip slip. Both planes trend subparallel to the bathymetric trend, so we are unable to distinguish the fault plane. We have chosen the steeper west-dipping plane because it would reach the sea bottom close to the northern end of the Puysegur Trench (Fig. 2), whereas the shallower dipping nodal plane would represent a fault that would outcrop about 20 km to the west of Resolution Ridge, in an area where there is no known evidence for active faulting. In either case the slip vector is oriented north to north–northwest, at a high angle (49°) to the predicted plate motion but perpendicular to the local strike of the Puysegur trench.

### (d) Deep Fiordland earthquake

The 1988 Te Anau earthquake (*K*) occurred at a depth of $60 \pm 5$ km within the Fiordland subduction zone, which strikes approximately 40° and dips about 80°, as defined by events deeper than about 50 km (Smith & Davey 1984). The steeply dipping plane in our mechanism (Fig. 7) strikes 281° (−10/+5°) which forms an angle of more than 20° to the long axis of the aftershock zone as determined by Reyners *et al.* (1991). Since our tests indicate that this discrepancy is greater than the uncertainties in our strike, it is possible that the aftershock locations are slightly biased. All the aftershocks located by Reyners *et al.* (1991) lie to the west

of the stations used in the locations. The closest stations used lie along a line trending north–northeast; such a network geometry will tend to introduce a bias in which the aftershock locations are elongate along a line perpendicular to this trend. Such a bias will also produce shallow depths for events located furthest from the stations; a phenomenon also observed in Fig. 5 of Reyners *et al.* (1991). If such elongation and depth bias is significant it may not be possible to prefer either of the fault planes using aftershock data, but horizontal movement on a shallow dipping plane (Fig. 7) at such depth seems less likely than a movement on the near-vertical plane as suggested by Reyners *et al.* (1991).

The slip vector from this focal mechanism is not expected to be useful for comparison with the plate-motion directions because of the depth of the event. Neither the *P*- nor *T*-axes, which for deeper events are thought to indicate internal stress orientation within a slab (Isacks & Molnar 1969), lie within the plane of the subducted slab (Fig. 7) as identified by Smith & Davey (1984) from seismicity, although the *T*-axis is close. This earthquake, therefore, represents deformation within the slab, as suggested by Reyners *et al.* (1991).

### (e) Normal faulting event

The 1965 April 11 earthquake at the western end of the Chatham Rise is unusual in that it is the only crustal normal-faulting event recognized in New Zealand apart from those associated with back-arc extension in the North Island (Smith & Webb 1986; Beanland, Blick & Darby 1990; Anderson, Smith & Robinson 1990). The choice of fault plane for this event was simplified by the recent recognition of south-dipping normal faults with an east–west strike that break the sea-floor on the northern flank of the Chatham Rise, and which appear to be reactivated faults bounding Cretaceous half-graben (Barnes 1991). We consider that this earthquake represents faulting on one of these south-dipping faults and so the slip vector is oriented south-east. This direction is roughly orthogonal to the predicted plate-motion direction.

### *P*-axes

In spite of the dramatically different focal mechanisms and slip vectors in the northern part of the South Island, the *P*-axes in that region are remarkably similar. The azimuths of the *P*-axes are plotted in Fig. 10. Since most of these events are either pure strike slip or pure reverse faulting, the subhorizontal nature of the *P*-axes means the azimuths are relatively well constrained.

The *P*-axis of any focal mechanism cannot be directly related to directions of principal stress (McKenzie 1969) but the very close agreement with the direction of the principal axis of shortening determined from repeated triangulation surveys (Bibby 1981, Fig. 10; Walcott 1984; Lamb & Bibby 1989) suggests that the seismic and aseismic deformation are both taking up the same motion. These results demonstrate that the strain is uniform throughout the area, although the displacements (slip) are markedly different on either side of the Alpine Fault. Similar results for different fault systems with a uniform strain field have been recognized in the North Island (Darby & Williams 1991).

### *SH* residuals

*SH* residuals are potentially useful for demonstrating lateral variations in crust and upper mantle structure (e.g. Molnar 1990). The residuals are determined for each station by the difference in the matched *SH* arrival time in the inversion results compared with that predicted by the standard traveltime tables. We have relocated all our events using *P* arrival times so their *P* residuals are small (generally less than 2 s), and consequently any significant *SH* residual is likely to be indicative of structure that has affected the propagation of shear waves.

The *SH* residuals derived from our inversion results are shown with the *SH* waveforms for each earthquake in Appendix A (on microfiche GJI 115/1). In almost all earthquakes, the *SH* residuals at Antarctic stations (SBA and SPA) were significantly delayed (mean 7.6, standard deviation 4.5), indicating a particular path effect. The orientation of the horizontal seismometers at SPA might contribute to such a residual if incorrectly aligned, however, the correct orientation has been confirmed by Okal (1992). For each event we determined the mean residual both including and excluding these stations (Table 3). The two earthquakes (*B* and *C*) at the southern end of the Hikurangi margin both show significant negative average *SH* residuals, probably because the take-off angle to most of the stations is down the Hikurangi subducted slab. Events in the central South Island show relatively small mean residuals (generally $<3$ s) with the exception of the deep Fiordland and Solander events.

## DISCUSSION

The purpose of our investigation was to improve the quality and number of fault-plane solutions of large earthquakes in the South Island, to aid the interpretation of the active tectonics. To facilitate this interpretation of the active tectonics we discuss groups of events by regions along the strike of the Australian–Pacific plate boundary.

### Northern South Island

The first two regions are north-east Marlborough and south-west Marlborough. The line dividing these regions (Fig. 11) is drawn on the basis of a distinct difference in the distribution of the deep seismicity, which, when extrapolated to the south-east, corresponds to a change in strike of the Marlborough Faults. The Awatere, Clarence and Hope faults all show a clear swing from an azimuth of 70–75° in south-west Marlborough, to 50° in the north-east (Bibby 1981). In fact many authors have taken this line to mark the end of the underlying subducted slab (e.g. Lamb & Bibby 1989; Ansell & Adams 1986). Recent data obtained since the improved seismograph coverage of this region show that this is not the case (Anderson *et al.* 1994). Fig. 12 shows cross-sections of the recent seismicity parallel and perpendicular to the margin. The section along strike clearly shows the transition from a deep slab in the north-east, with many events to 250 km depth, to a shallow slab with events to 100 km, and finally no activity below 50 km in the south-west. Both transitions appear to be too abrupt to be an artefact of moderate-depth events being restricted to

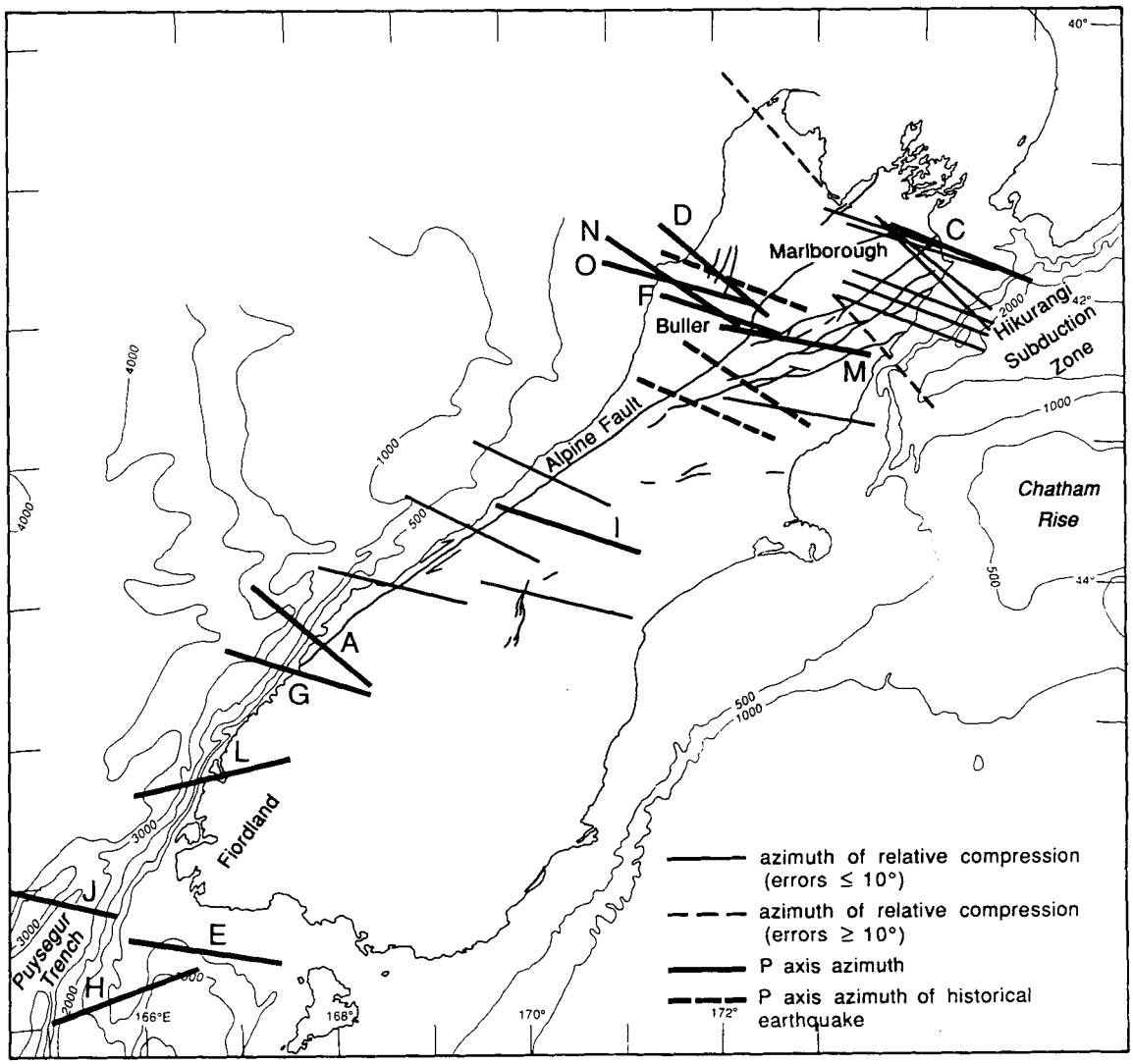


**Figure 10.** *P*-axis azimuths for all the events in this study compared with the azimuths of relative compression determined from geodetic data (Bibby 1981; Walcott 1984; Lamb & Bibby 1989). The Chatham Rise normal-faulting event is not included because its *P*-axis is subvertical and, therefore, the azimuth is poorly defined.

crustal depths during routine analysis. The sections perpendicular to the strike of the plate boundary show a pronounced extra 150 km of slab to the north-east. It is important to note that the shallow part of slab common to both sections is identical within the accuracy of the routine locations. The north-east section is distinguished only by the extra steeply dipping piece of slab; the shallow part does not dip more steeply than the section to the south-west, nor is it deeper. The tear in the slab identified by Robinson (1986) further to the north-east has a depth difference across it of about 6 to 7 km. Such a difference would not be distinguishable with the catalogue data that we have used.

Note that the extension of the dividing line to the south-east intersects the end of the 2000 m bathymetric contour in the Hikurangi Trough, which roughly marks the beginning of the transition from the subduction of oceanic (or possibly thinned continental, Davy 1992) crust to convergence of continental crust (Walcott 1978; Bibby 1981).

*North-east Marlborough*

Bibby (1981) analysed the geodetic data for the north-east Marlborough region and found that strain was partitioned between strike-slip faulting inland to the north-west, and reverse faulting on land nearer to the Hikurangi Trough (i.e. trenchward). Such partitioning of oblique convergence at subduction zones is not unusual (Fitch 1972; Jarrard 1986), and is the southern extension of partitioning observed in the North Island, New Zealand (Walcott 1984; Robinson 1994). Lamb (1988), and Lamb & Bibby (1989) suggest that the entire north-east Marlborough system is rotating clockwise through the translation and rotation of large crustal blocks.

The only earthquake that occurred in the north-east Marlborough region (*C*) has a centroid depth of 19 km, which places it in the crust above the subducted Pacific Plate, according to the cross-section of Robinson (1986). The mechanism of event *C* is oblique, with the horizontal

**Table 3.** *SH* residuals determined from match of observed and synthetic waveforms.

| Date | Event | SH residual excluding SBA/SPA | | | SH residual including SBA/SPA | | |
|---|---|---|---|---|---|---|---|
| | | x | s | n | x | s | n |
| 640308 | A | 1.8 | 0.8 | 3 | 4.4 | 5.2 | 4 |
| 650411 | B | -6.2 | 2.0 | 4 | -4.1 | 5.0 | 5 |
| 660423 | C | -2.9 | 1.7 | 7 | – | – | |
| 680523 | D | 0.0 | 1.7 | 6 | 2.8 | 5.5 | 8 |
| 680925 | E | 6.7 | 4.5 | 9 | 7.9 | 5.6 | 10 |
| 710813 | F | 2.5 | 1.6 | 5 | 4.1 | 4.3 | 6 |
| 760504 | G | 2.8 | 2.0 | 9 | 3.6 | 2.7 | 11 |
| 791012 | H | 0.6 | 3.3 | 10 | 0.5 | 3.2 | 12 |
| 840624 | I | -0.4 | 1.5 | 8 | 0.4 | 2.8 | 9 |
| 850131 | J | 2.7 | 2.0 | 19 | – | – | |
| 880603 | K | 6.2 | 2.3 | 13 | 6.3 | 2.3 | 14 |
| 890531 | L | 3.1 | 2.5 | 18 | 3.3 | 2.6 | 19 |
| 900210 | M | 1.1 | 2.8 | 17 | 1.8 | 3.8 | 18 |
| 910128;1 | N | 0.8 | 3.7 | 7 | – | – | |
| 910128;2 | O | 3.1 | 3.9 | 7* | – | – | |

* excluding value at CTAO
x = mean
s = standard deviation
n = number.

projection of the slip vector in the direction of plate motion. This direction does not agree with that predicted by the block model of Lamb & Bibby (1989) (velocity $U_{AB}$ in their Fig. 21), which would be north-west. Nor does event *C* show any evidence of the strain partitioning found in the geodetic data by Bibby (1981). There are two possible reasons for this. First, if the partitioning observed by Bibby (1981) is a gradual transition from strike-slip inland to reverse as we approach the Hikurangi Trough, a part of the way across this transition we might expect oblique-faulting solutions such as event *C* (i.e. no partitioning on a local scale). The location of event *C* in the middle of the deforming zone may be compatible with such a model (Fig. 11). Secondly, event *C* is 19 km deep. Both the geodetic strain partitioning and block rotations are observed at the surface, which is compatible with simple oblique deformation in the direction of plate motion at greater depths.

The Marlborough Faults in the north-east region are not ideally oriented for strike-slip faulting in the direction of plate motion (259°). The overall pattern here is thus one of oblique convergence being accommodated by strike-slip movement away from the trench, with the shortening accommodated trenchward by reverse and oblique movement on the north-easterly oriented Marlborough Faults. The residual reverse component is manifest by the uplift of the Kaikoura Ranges, as pointed out by Bibby (1981).

*South-west Marlborough*

Bibby (1981) suggested that the strain partitioning he observed to the north-east did not continue to the south-west, because the faults in this region are more favourably oriented to accommodate all of the plate motion. This motion should be dominantly strike-slip, with little reverse component or uplift. Lamb & Bibby (1989) noted a change to less uplift in the south-west region, consistent with a transition to a dominantly strike-slip regime.

Our results indicate that, while there is right-lateral strike-slip faulting in the south-west Marlborough region, there is also reverse faulting with a NE strike further inboard of the margin, near Buller (Fig. 8). Focal mechanisms on these two types of faults have similar *P* axes (Fig. 10), but very different slip vectors. The average slip vector for the three strike-slip events (*F, I, M*) is 237 ± 2°, and for the three reverse-faulting events in Buller (*D, N, O*) is 297°. In this region, the direction of Pacific–Australia plate convergence predicted by the model NUVEL-1 (DeMets *et al.* 1990) is 255°. Thus the slip vectors on the reverse faults are significantly (40°) clockwise of the expected direction of relative plate motion, while those on the strike-slip faults are slightly anticlockwise of the plate motion.

One explanation for the shortening in the Buller region is that the Pacific–Australia plate motion is again partitioned between strike-slip and reverse faulting, but here with strike-slip faulting in Marlborough and reverse faulting in Buller; an opposite polarity to that observed in north-east Marlborough. The rate of shortening required to achieve this partitioning is small. If we take the 18° discrepancy between the plate-motion direction and the average direction of slip on the strike-slip faults, the necessary rate of shortening in the Buller region perpendicular to the

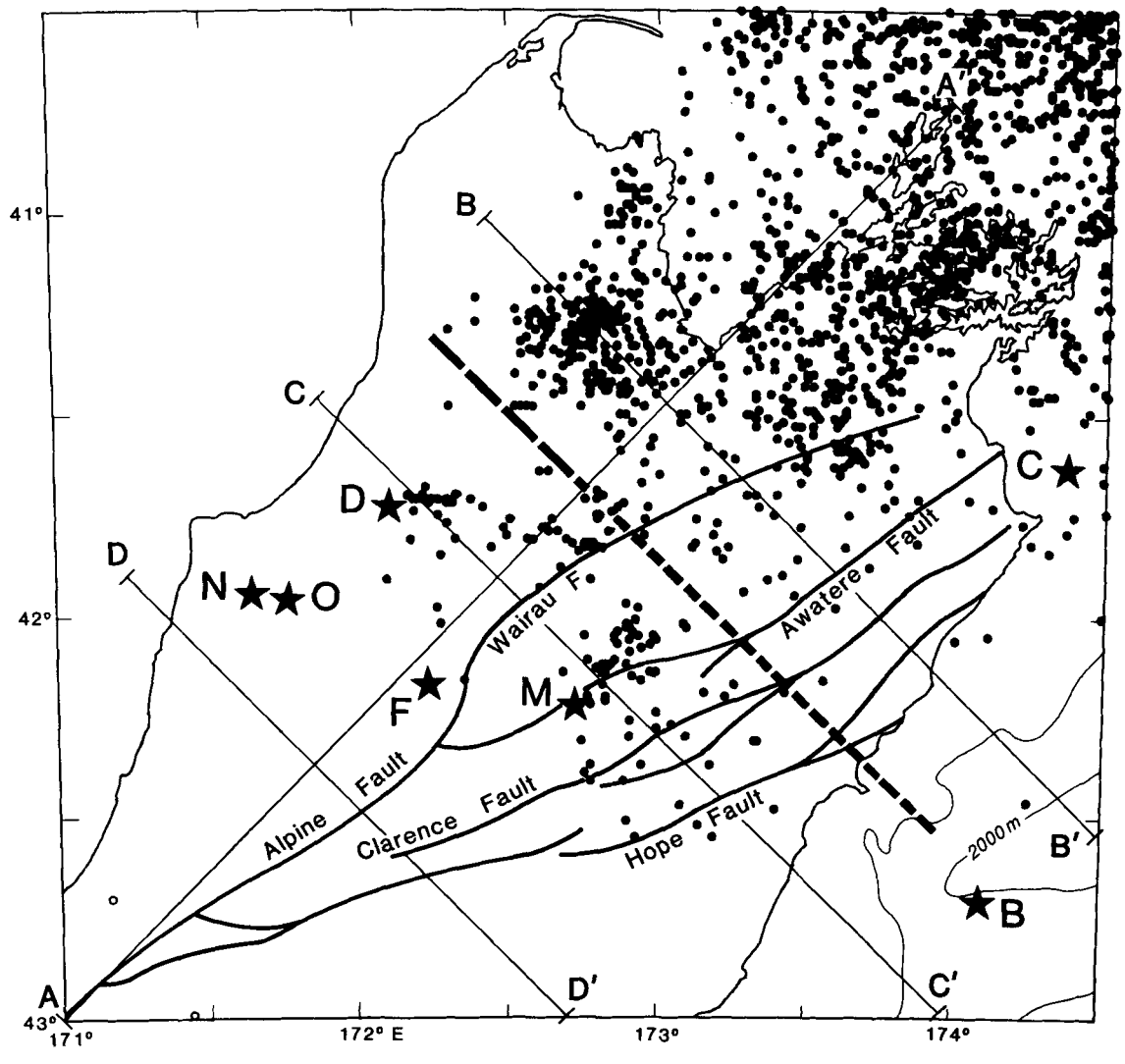


**Figure 11.** Subcrustal (depth > 50 km) seismicity of the northern South Island recorded by the New Zealand national network from January 1990–May 1992 (magnitude >2.0). Cross-section lines indicate profiles shown in Fig. 12. Heavy dashed line delimits the two different segments of the Benioff Zone. If extrapolated towards the south-east, this line also coincides with a marked change in strike of faults in the Marlborough Fault System that appears to delimit two separate regions whose style of deformation (e.g. partitioning) vary. These regions, north-east and south-west Marlborough, are discussed in the text. Locations of earthquakes considered in this paper are marked stars. The 2000 m isobath approximates the continental margin.

strike-slip faults would be only 12 mm $yr^{-1}$ (40 mm $yr^{-1}$ × sin 18°) whereas the rate of strike-slip faulting in Marlborough would be 38 mm $yr^{-1}$. This relatively low rate of shortening in the Buller region would require a moment release rate of about $5.0 \times 10^{17}$ Nm $yr^{-1}$ in a zone 100 km long and 10 km thick if it were all accommodated seismically: in other words, an earthquake of the 1968 Inangahua ($D$) size about every 100 yr, or one of the 1929 Murchison size about every 1000 yr. The time interval over which quantitative seismological observations are available is too short to have confidence in using seismic moment release rates to estimate the absolute rates of seismic shortening and strike-slip motion for the Buller and Marlborough regions. However, it is clear from geological observations in the Marlborough region, that the slip rates on the main faults of the Marlborough system (the Clarence, Hope and Awatere faults) are relatively high (up to 20–25 mm $yr^{-1}$), and can probably account for most of the expected plate motion (Berryman *et al.* 1993; Lamb & Bibby 1989; van Dissen & Yeats 1991). We expect that the greater seismic activity of the Buller region this century is an anomaly related to the short-observation period, and that larger though relatively infrequent earthquakes occur on the Marlborough Fault System.

### *Partitioning of strike-slip and reverse faulting*

If partitioning of strike-slip and reverse faulting occurs in the manner suggested above, it has some peculiarities. First, the slip vectors on the reverse and strike-slip faults are not orthogonal. In several continental regions where partitioning is thought to occur, the two sets of slip vectors are approximately orthogonal (e.g. Mount & Suppe 1987; Abers & McCaffrey 1988; Jackson & Molnar 1990; Jackson 1992).

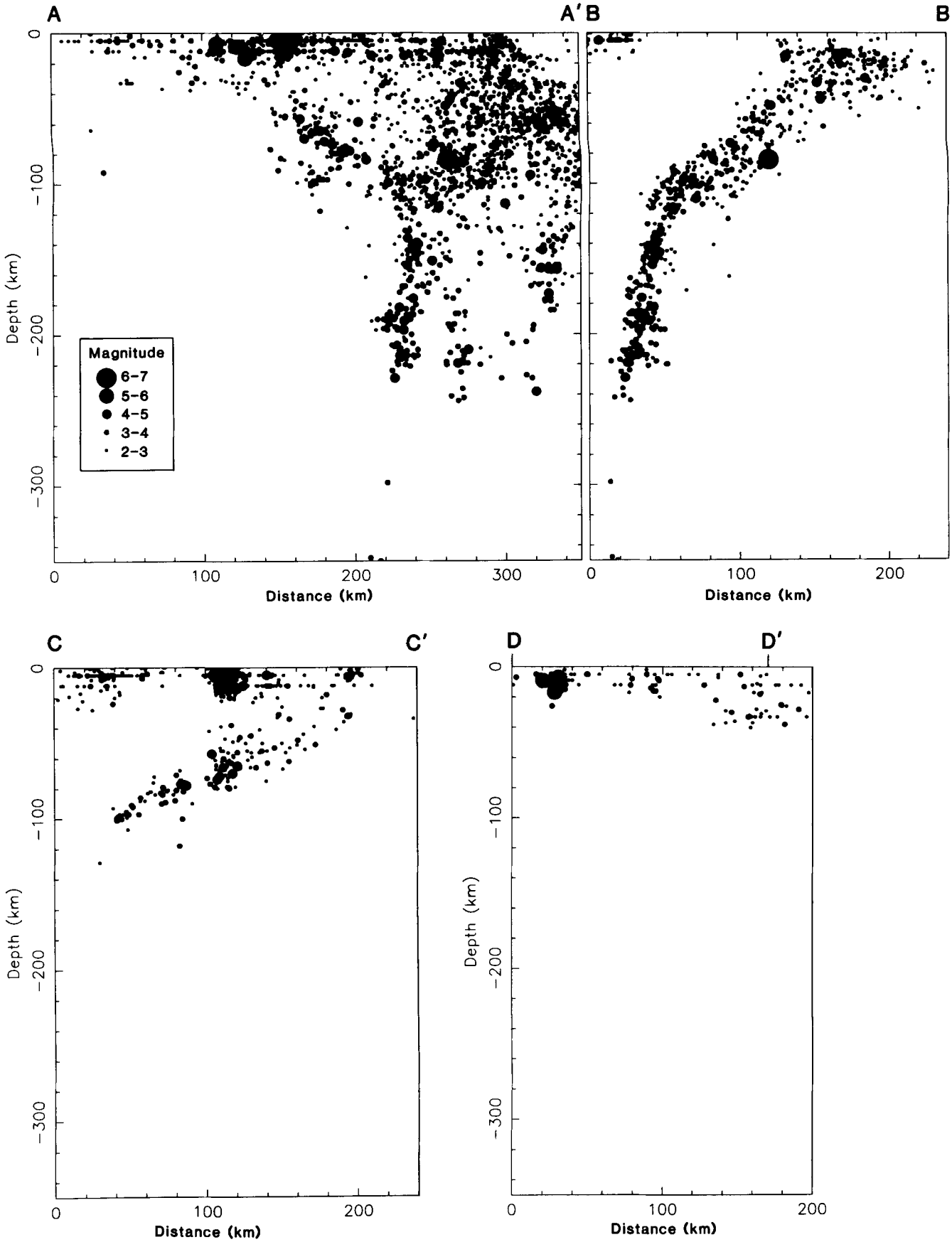


**Figure 12.** Cross-sections of subcrustal seismicity shown in Fig. 11. The projection width for cross-section AA′ is 100 km and is 34 km for BB′, CC′, DD′, thus including all events whose epicentres occur on Fig. 11. Section AA′ shows that the deepest events occur in the north and there is a sharp truncation of the deepest seismicity. Comparison of sections BB′ and CC′ shows that the Benioff Zone has a similar dip in both to depths of about 100 km, but below this, they are dramatically different in that the northern section (BB′) has a very steeply dipping extension to depths of about 250 km, but the southern section (CC′) appears to terminate abruptly.

However, there is no particular reason why they should be orthogonal, and there are exceptions, even in island arcs (e.g. Ekstrom & Engdahl 1989). McCaffrey (1992) discusses the nature of partitioning in island arcs, where the strike slip and thrust faults are often parallel to each other and to the trench. In the northern part of the South Island of New Zealand, the strike-slip faults of Marlborough are not parallel to the reverse faults in Buller. We suspect this is because the Buller faults are reactivated normal faults of pre-Oligocene age (Nathan *et al.* 1986). Secondly, in most other partitioned systems, the thrust faulting is trenchward of the strike-slip faulting, in contrast to that observed here. We believe that the switch in the polarity of the partitioning is due to subduction being impeded in southern Marlborough, because of the presence of the relatively buoyant Chatham Rise. In the southern region the shortening across the margin is accommodated by reactivating normal faults of pre-Oligocene age in the Buller region as reverse structures (Gage 1952; Nathan *et al.* 1986). Crustal shortening of 25 km across the 100 km wide zone has been determined from the average height of the Nelson tectonic zone (taken to represent the uplift) by Walcott (1978).

### *Consequences of a partitioning model*

Since the Marlborough strike-slip system is south-east of the crustal shortening occurring in Buller, these faults must be transported north-westwards relative to the Alpine Fault further to the SW. This process could have formed the bend in the Alpine Fault, whose present amplitude of about 15 km could grow in just 1.3 Myr if the rate of shortening in Buller is 12 mm $yr^{-1}$. This geometry, which was recognized by Walcott (1978), resembles that in eastern Turkey and the Caucasus in western Asia (Jackson 1992).

A possible geological evolution is illustrated schematically in Fig. 13. Suppose that the Alpine Fault, when it initially formed, accommodated all the plate motion. Since the inception of the Alpine Fault as a transform structure, the pole of rotation describing the relative motion of the Australian and Pacific plates has shifted south (Walcott 1978; Stock & Molnar 1982) and the component of convergence has increased. This convergence could not be taken up near the margin because of the presence of buoyant material of the Chatham Rise. However, the pre-existing normal faults in the Buller region could be reactivated as reverse faults to accommodate the increasing compressional component, leaving the strike-slip component to be taken up on the Alpine Fault, which then began to migrate NW, forming the bend. As the strike-slip faults are transported NW they become less active as strike-slip motion is transferred to newer faults forming to the south-east, in an attempt to keep the Alpine Fault in the central south Island as a through-going structure. This evolution would leave the Alpine Fault in this region with a lower slip rate than further south in its central section, because it is no longer the dominant active fault.

This hypothesis is consistent with the different observed slip rates of $25 \pm 10$ mm $yr^{-1}$ on the central and southern sections of the Alpine Fault compared with $10 \pm 2$ mm $yr^{-1}$ in the area close to the Big Bend (Berryman *et al.* 1994). It also accounts for the Quaternary slip rate on the Wairau fault (the continuation of the Alpine Fault NE of the bend)

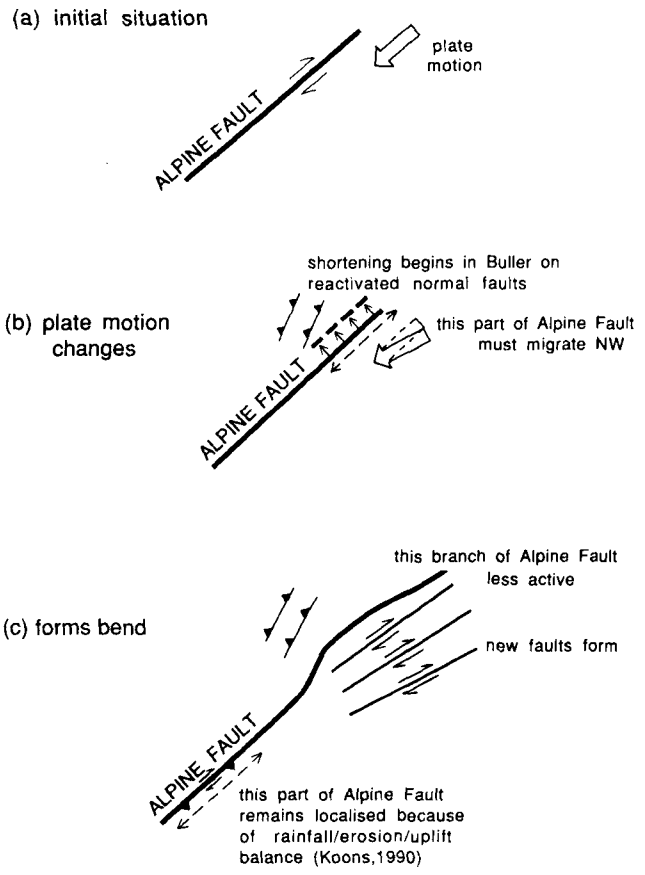


**Figure 13.** Sketch map showing proposed evolution of fault systems in the northern South Island.

being lower than that of most of the Marlborough faults to the SE and only about 25 per cent of that on the Hope Fault (van Dissen & Yeats 1991).

Geological, geodetic and palaeomagnetic aspects of the deformation in Marlborough are discussed in detail by Lamb (1988, 1989) and Lamb & Bibby (1989). Our suggestions are not in conflict with the kinematic models they propose, but modify them, in that the entire Marlborough system must be migrating NW relative to the central Alpine Fault and Australian plate.

## The role of subduction

Earlier in this section we discussed the structure of the subduction zone (Figs 11 and 12). It is clear that a discontinuity in the zone of subcrustal earthquakes is associated with the change in strike of the Marlborough faults, the change in polarity of the partitioning of the strain, and the shallowing of the Hikurangi Trough to less than 2000 m, which marks the beginning of the transition to continent–continent collision in the South Island. How are these observations related?

First, we do not believe that the width or nature of the deformation in the south-west Marlborough region is directly controlled by tractions on the (shallow dipping) plate interface. In the Buller region the plate interface is about 100 km deep. Thus, the stresses driving the deformation in that region must be transmitted through

the lithosphere from the plate boundary, not from the subducted slab 100 km below. Secondly, we do not think that the different slab lengths below the two Marlborough regions have been caused by different rates of subduction. The required lateral offset in the subducted plate of 150 km would have more pronounced effects at the surface than just a minor deflection of the Marlborough faults. Instead, we suggest that the different slab lengths were original, and reflect the geometry of the margin when subduction initiated (Fig. 12). This is essentially the model of Lamb & Bibby (1989), which requires a large rotation of the northern margin from the early Miocene that was caused by the arrival of the continental rocks of the Chatham Rise (Walcott 1978). The existence of a slab under south-west Marlborough, which was assumed to be aseismic because its structure could not be resolved with the available seismological data was predicted by Lamb & Bibby (1989). As we have already discussed, the lengths are the only resolvable difference in the two parts of the slab.

Thus it is the transition from oceanic to continental crust that is important, together with the presence of the Buller basins whose associated normal faults were favourably oriented from a kinematic viewpoint, to be reactivated as reverse structures. These two factors have caused the different style of partitioning in south-west Marlborough.

### The Alpine Fault and Fiordland

The two well-constrained focal mechanisms in northern Fiordland (*G, L*) are compatible with oblique right-lateral strike-slip and reverse motion on the Alpine Fault, with slip vectors that are not resolvably different from the expected plate motion. Geological observations suggest that most of the plate motion is probably accommodated on or near the Alpine Fault in this region (Norris *et al.* 1990). Although active faulting certainly extends 200 km farther SE into central and coastal Otago, (e.g. Berryman & Beanland 1991; Yeats 1987; Beanland & Berryman 1989) these faults probably account for much less of the present-day motion than does the faulting along the west coast. Thus, although the deformation at this latitude is distributed, most of the motion is concentrated in a narrow zone along the west coast. It is therefore not surprising that the earthquakes show the oblique convergent mechanisms with slip vectors close to the plate-motion direction. This is an important contrast with the northern South Island, where the faulting is genuinely distributed over many comparably active faults that extend over a region around 200 km in width. In continental collision zones elsewhere in the world, shortening is nearly always distributed over wide regions (e.g. Molnar & Tapponnier 1975; Jackson & McKenzie 1984), and this is now understood as a natural consequence of the buoyancy forces that arise from crustal thickening, which make the deformation migrate away from the high ground as plateaus and mountains grow (e.g. Houseman & England 1986). It is thus the localized deformation on the central and SW coast of the South Island that is unusual in this respect. We suspect that the reason for the contrast between this region and the northern South Island is that suggested by Adams (1980) and further developed by Koons (1989, 1990), namely that the high rainfall on the west and south-west coast allows erosion to remove material as the crust is thickened, thereby preventing the buoyancy forces from distributing the deformation, whereas the lower rainfall and erosion in the NE has allowed the deformation to become distributed in a more typical fashion.

### Puysegur region

The Resolution Ridge earthquake (*J*) remains a mystery; it lies to the west of the seismicity accompanying the Puysegur subduction zone, and its slip vector is significantly rotated from the plate-motion direction.

The tectonic setting of Resolution Ridge is unclear. The Puysegur event (*H*) that occurred less than 100 km to the south-east of it was related to thrusting in the Puysegur Trench. It is possible that Resolution Ridge is a segment of the Macquarie Ridge Complex, which is made up of a series of isolated ridges and trenches (Anderson 1990). However, gravity data show that Resolution Ridge appears to be the northern end of a more elongate ridge system that trends towards the southwest (Davy 1989). The Resolution Ridge earthquake may therefore represent obduction of this ridge as it encounters the New Zealand continental shelf and the active plate boundary. An analogy for such a tectonic setting is the Gorringe Ridge, which is a block of oceanic crust and upper mantle that rises almost 4000 m from the deep sea-floor in the plate boundary zone between Africa and Eurasia (Souriac 1984). Several reverse-faulting earthquakes have occurred beneath that ridge with centroid depths up to 50 km (Fukao 1973; Grimison & Chen 1986), although the largest recent event ($M_S$ 7.9) has been shown to be a multiple event with both centroid depths at about 30 km (Grimison & Chen 1988). The reverse-faulting mechanisms suggest that the Gorringe Ridge is actively obducting. Both Gorringe and Resolution ridges are in comparable plate-boundary settings and both have relatively deep reverse-faulting events associated with them.

Another possible explanation for the Resolution Ridge earthquake is that it is related to the bending of the Australian plate as it enters the Puysegur subduction system. Outer rise extension earthquakes occur at relatively shallow depths (<25 km, Forsyth 1982) whereas deeper events are expected to have thrusting mechanisms. The Resolution Ridge earthquake, with a centroid depth of 27 km (−12/+8 km) could represent a deeper bending earthquake.

The two most southern events in our study are close together but have pure strike-slip and pure dip-slip mechanisms. The 1979 Puysegur (*H*) earthquake represents active subduction on an east-dipping thrust. The 1968 Solander (*E*) earthquake is a strike-slip event that probably occurred on the off-shore extension of the Fiordland Boundary Fault Zone, which is imaged on seismic sections as an active feature that offsets the sea-floor (Grant 1985). If this fault is active in its onshore extension as a dextral strike-slip fault, then it may help in explaining the rapid uplift of the Fiordland region (between 1.1 and 5.4 mm $yr^{-1}$ in southern Fiordland; Ward 1988; Bishop 1985, 1991). If the Fiordland Boundary Fault Zone has been active as a significant dextral strike-slip fault then it has probably overlapped the southern extension of the Alpine Fault and

thus formed a compressional step-over in a dextral strike system; a geometry that results in uplift of the intervening crustal block.

### Normal faulting on the Chatham Rise

The 1965 Chatham Rise earthquake (*B*) is an important event because it demonstrates that normal faulting is occurring at the southern limit of the Hikurangi trench. The explanation for a normal-faulting earthquake in this tectonic setting could be that the event represents bending of the downgoing slab (Christensen & Ruff 1983) but the recognition of active normal faults on the north flank of the Chartham Rise that have the same strike and dip direction as the south-dipping nodal plane (Barnes 1991) suggests that the extension in this region has occurred on reactivated faults. These faults are at a high angle to the Hikurangi margin and the Marlborough Fault System, which suggests that they are not directly related to plate bending.

A possible explanation for the occurrence of normal faulting in this region is that it is a consequence of a minor amount of buckling at the northern end of the southern Marlborough strike-slip system. A tentative model for the kinematics of such an interaction is shown in Fig. 14. As buckling occurs in the region where the Marlborough faults change strike, the continental crust of the Chatham Rise is rotated clockwise and faults in that region would show normal-faulting movement with a small component of left-lateral strike-slip as in the Chatham Rise earthquake (*B*); a model analogous with the normal faulting in the Aegean Sea (Taymaz, Jackson & McKenzie 1991). In this model the strike-slip faults in south-west Marlborough take up most of the plate motion, the reverse faults in the Buller–Nelson region take up nearly all the rest and the normal faulting and buckling on the Chatham Rise are probably of only minor significance. In essence, the normal faulting represents slivers of the Chatham Rise being spalled off as the Chatham Rise slides past southern Marlborough.

## CONCLUSIONS

The focal mechanisms of 15 large earthquakes in the South Island region show differing modes of accommodating the Australian–Pacific plate motion. In the northern South

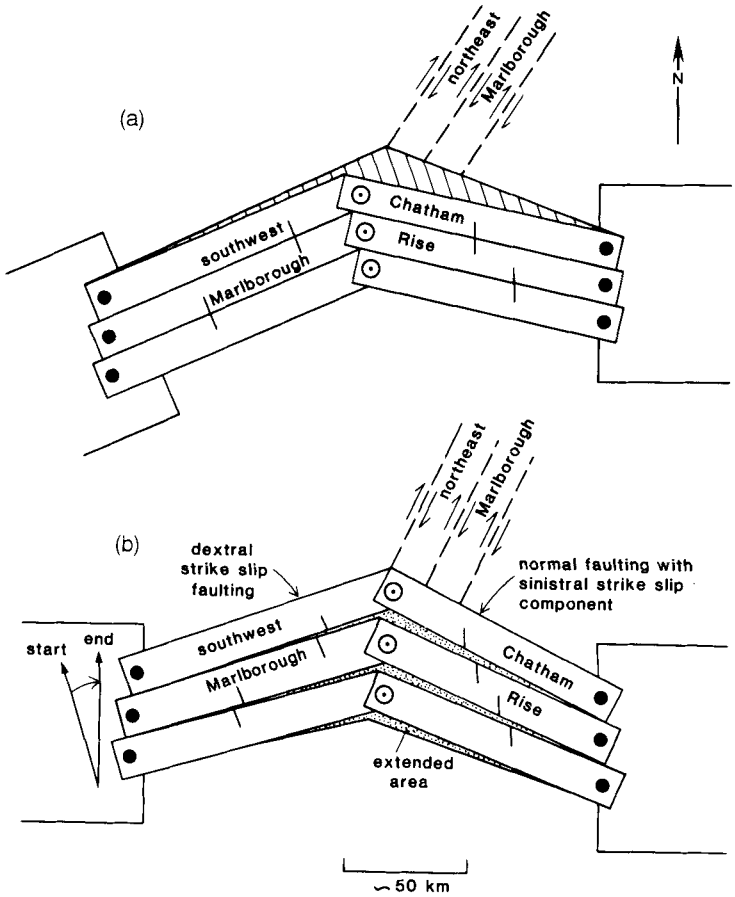


**Figure 14.** Sketch of a simple model for the Marlborough Fault System–Chatham Rise that illustrates how east–west shortening may be achieved by buckling. This model involves two sets of slats that are in relative motion and can easily be constructed from cardboard. Solid circles are pivots (screws) attached to the rigid (non-deforming) blocks to either side. The open circles are screws joining two slats, but which are otherwise free to move. The configuration in (a) moves to (b) following a clockwise rotation of the left-hand margin (south-west Marlborough) which represents a distributed right-lateral shear of the SW Marlborough Fault System. In this illustration, the right-hand pivots (attached to the Chatham Rise) do not rotate. The stippled region in (b) represents new surface area created by extension. The model should not be taken literally: it is designed to show oblique left-lateral and normal faulting that dies out eastwards. The Chatham Rise rotates clockwise and so can contribute in a minor way to the E–W shortening. A similar model to explain the way in which the Marlborough faults move was proposed by Merzer & Freund (1974) although our model expands their concepts to include normal faulting in the Chatham Rise.

Island the deformation is partitioned and distributed over a region up to 200 km wide, whereas in the southern South Island the largest earthquakes are confined to a narrower zone in which the motion is compatible with that predicted for the plate motion.

In the northern South Island there are two distinct seismotectonic provinces; in north-east Marlborough geodetic data and geological mapping (Lamb 1988, 1989; Lamb & Bibby 1989) suggests that deformation is partitioned into onshore strike-slip and offshore reverse faulting. Our only focal mechanism that occurs within this province indicates oblique-slip faulting which is compatible with the plate-motion direction. A line which marks the southern boundary of this region coincides with the change in strike of the Marlborough faults and also appears to be related to a change in the original geometry of the subducting plate as it is now manifest in the Benioff zone.

In the south-west Marlborough–Buller region the focal mechanisms fall into two distinct groups with almost pure dip-slip reverse mechanism occuring in the Buller region, and dominantly strike-slip mechanisms in the Marlborough Fault System. We suggest that this partitioning of deformation has resulted from a changed plate-motion direction which required a component of shortening to be accommodated. This shortening could not be taken up in the offshore (eastern) region because of the presence of the relatively buoyant Chatham Rise, but was taken up in the Buller region on pre-existing normal faults that were reactivated as reverse faults in the Late Oligocene–Early Miocene. Accommodation of the convergence in the Buller region resulted in the north-westwards deflection of the Alpine Fault in this region. New strike-slip faults developed in the Marlborough Fault System, possibly in an attempt to keep the Alpine Fault as a through-going feature. In the central South Island one strike-slip earthquake that lies to the east of the Alpine Fault probably represents movement on the southernmost fault of the Marlborough Fault System.

At the southern end of the Alpine Fault deformation occurs as oblique-slip faulting within a relatively narrow zone that probably marks the transition of the major strike-slip fault to a shallower dipping structure delimiting the subduction of the Australian plate beneath the Pacific plate. The continuation of this subduction to the south is marked by the 1979 Puysegur earthquake that had a dominantly reverse-faulting mechanism. Two unexpected focal mechanisms occurred in this southern offshore region; the first was a relatively deep (27 km) event to the west of the Puysegur subduction system. This earthquake occurred near Resolution Ridge and its mechanism suggests that the ridge is obducting as it encounters the Puysegur–Fiordland subduction zone. The other unusual mechanism was a strike-slip event that probably occurred on the offshore extension of a major recently active strike-slip fault. This earthquake may be indicative of other large events on this dextral strike-slip fault whose overlapping geometry with the southern continuation of the Alpine Fault may be an explanation for the high uplift rates of the Fiordland block.

The only normal faulting event that we determined occurred beneath the northern edge of the Chatham rise in an area where active normal faults have been identified from shallow seismic data. We suggest that the normal faulting in this region results from a complex interaction of the Chatham Rise with the faults of the Marlborough Fault System.

## ACKNOWLEDGMENTS

We are grateful to Madeline Zirbes, Brian Ferris, June Pongratz and Jim Taggart for helping us get all the data together for this paper. Carolyn Hume's draughting work is especially appreciated. We thank our colleagues Sarah Beanland, Huntly Cutten, Rick Sibson, Dick Walcott, Dick Norris, Moses Turnbull and Graham Bishop for sharing their knowledge of New Zealand tectonics with us. This paper was reviewed by our colleagues, Hugh Bibby and Martin Reyners. We thank Rick Sibson and an anonymous reviewer for their particularly constructive comments. This paper is Institute of Geological and Nuclear Sciences contribution number 13, and Cambridge Earth Sciences contribution 3090.

## REFERENCES

Abers, G. & McCaffrey, R. 1988. Active deformation in the New Guinea fold-and-thrust belt: seismological evidence for strike-slip faulting and basement-involved thrusting, *J. geophys. Res.* **93,** 13 332–13 354.

Adams, J., 1978. Late Cenozoic erosion in New Zealand, *PhD thesis,* Victoria University of Wellington.

Adams, J., 1980. Contemporary uplift and erosion of the Southern Alps, New Zealand, *Geol. Soc. Am. Bull.* **91,** 1–114.

Adams, R. D., 1970. Seismological studies of the Seddon earthquake, 1966, *Bull. N.Z. Dept Sci. Indust. Res.*, **199,** 5–14.

Anderson, H. J., 1990. The 1989 Macquarie Ridge earthquake and its contribution to the regional seismic moment budget, *Geophys. Res. Lett.* **17,** 1013–1016.

Anderson, H. J., 1991. Focal mechanisms of some recent large New Zealand earthquakes, *N.Z. J. Geol. Geophys.* **34,** 103–109.

Anderson, H., Smith, E. & Robinson, R., 1990. Normal faulting in a back arc basin: seismological characteristics of the March 2, 1987, Edgecumbe, New Zealand earthquake, *J. geophys. Res.* **95,** 4709–4723.

Anderson, H., Beanland, S., Blick, G., Darby, D., Downes, G., Haines, J., Jackson, J., Robinson, R. & Webb, T., 1993. The 1968 May 23 Inangahua, New Zealand, earthquake: an integrated geological, geodetic and seismological source model, *N.Z. J. geol. Geophys.*, in press.

Ansell, J. & Adams, D., 1986. Unfolding the Wadati–Benioff zone in the Kermadec–New Zealand region, *Phys. Earth planet. Inter.* **44,** 274–280.

Arabasz, W. J. & Robinson, R., 1976. Microseismicity and geologic structure in the northern South Island, New Zealand, *N.Z. J. Geol. Geophys.*, **19,** 569–601.

Barnes, P., 1991; Active extension within the transpressive southern Hikurangi margin: the north Mernoo fault zone—some preliminary results and interpretation, *Geol. Soc. N.Z.*, **56,** 6–8.

Beanland, S., 1987, Field guide to sites of active deformation: South Island, New Zealand, *N.Z. geol. Surv. Record* **19.**

Beanland, S. & Berryman, K., 1989. Style and episodicity of late Quaternary activity on the Pisa–Grandview Fault Zone, Central Otago, New Zealand, *N.Z. J. Geol. Geophys.*, **32,** 451–461.

Beanland, S., Blick, G. H. & Darby, D. J., 1990. Normal faulting

in a back arc basin: geological and geodetic characteristics of the 1987, Edgecumbe earthquake, New Zealand, *J. geophys. Res.*, **95,** 4693–4707.

Berryman, K., 1979. Active faulting and derived PHS directions in the South Island, New Zealand, *R. Soc. N.Z. Bull.*, **18,** 29–34.

Berryman, K. R. 1980. Late Quaternary movement on White Creek Fault, South Island, New Zealand, *N.Z. J. Geol. Geophys.* **23,** 93–101.

Berryman, K. & Beanland, S., 1991. Variations in fault behaviour in different tectonic provinces of New Zealand, *J. struct. Geol.*, **13,** 177–189.

Berryman, K. R., Beanland, S., Cooper, A. F., Cutten, H. N., Norris, R. J. & Wood, P. R., 1993. The Alpine Fault, New Zealand: variation in Quaternary structural style and geomorphic expression, *Ann. Tecton.* in press.

Bibby, H. M., 1981. Geodetically determined strain across the southern end of the Tonga–Kermadec–Hikurangi subduction zone, *Geophys. J. R. astr. Soc.*, **66,** 513–533.

Bishop, D. G., 1985. Inferred uplift rates from raised marine surfaces, southern Fiordland, New Zealand, *N.Z. J. Geol. Geophys.*, **28,** 243–251.

Bishop, D. G., 1991. High-level marine terraces in western and southern New Zealand: indicators of the tectonic tempo of an active continental margin, *Spec. Publ. Int. Ass. Sediment.* **12,** 69–78.

Chase, C. G., 1978. Plate kinematics: the Americas, East Africa and the rest of the world, *Earth planet. Sci. Lett.*, **37,** 355–368.

Christensen, D. H. & Ruff, L. J., 1983. Outer-rise earthquakes and seismic coupling, *Geophys. Res. Lett.*, **10,** 697–700.

Cooper, A. F. & Norris, R. J., 1990. Estimates of the timing of the last coseismic displacement on the Alpine Fault, northern Fiordland, New Zealand, *N.Z. J. Geol. Geophys.*, **33,** 303–307.

Cowan, H. A., 1990. Late Quaternary displacements on the Hope Fault at Glynn Wye, North Canterbury, *N.Z. J. Geol. Geophys.* **33,** 285–293.

Cowan, H. A., 1991. The North Canterbury earthquake of September 1, 1888, *J. R. Soc. N.Z.*, **21,** 1–12.

Cutten, H. N. C., 1979. Rappahannock Group: Late Cenozoic sedimentation and tectonics contemporaneous with Alpine Fault movement, *N.Z. J. Geol. Geophys.* **22,** 535–553.

Darby, D. J. & Williams, R. O., 1991. A new geodetic estimate of deformation in the Central Volcanic Region of the North Island, New Zealand, *N.Z. J. Geol. Geophys.*, **34,** 127–136.

Davey, F. J. & Broadbent, M., 1980. Seismic refraction measurements in Fiordland, southwest New Zealand, *N.Z. J. Geol. Geophys.*, **23,** 395–406.

Davey, F. J. & Smith, E. G. C., 1983. The tectonic setting of the Fiordland region, south-west New Zealand, *Geophys. J. R. astr. Soc.*, **72,** 23–38.

Davey, B. W., 1989. *Southern Oceans Sheet 1*, Gravity anomaly map, miscellaneous series, 1:4,000,000, Department of Scientific & Industrial Research, Wellington, New Zealand.

Davey, B. W., 1992. The influence of subducting plate buoyancy on subduction of the Hikurangi–Chatham Plateau beneath the North Island, New Zealand, *Am. Ass. Petrol. Geol.*, Memoir **53,** Advances in the Geology and Geophysics of the Continental Margin.

DeMets, C., Gordon, R. G., Argus, D. F. & Stein, S., 1990. Current plate motions, *Geophys. J. Int.* **101,** 425–478.

Dowrick, D. J., 1991. Magnitude reassessment of New Zealand earthquakes, *Earthq. Eng. struct. Dyn.*, **20,** 577–590.

Dowrick, D. J. & Smith, E. G. C., 1990. Surface wave magnitudes of some New Zealand earthquakes 1901–1988, *Bull. New Zealand Nat. Soc. Earthq. Eng.*, **23,** 198–219.

Dziewonski, A. M., Chou, T. A. & Woodhouse, J. H., 1981. Determination of earthquake source parameters from waveform data for studies of global and regional seismicity, *J. geophys. Res.*, **86,** 2825–2852.

Dziewonski, A. M., Ekstrom, G., Franzen, J. E. & Woodhouse, J. H., 1987. Global seismicity of 1979: centroid–moment tensor solutions of 524 earthquakes, *Phys. Earth planet. Inter.*, **48,** 18–46.

Eiby, G. A., 1978. The Milford Sound earthquake of 1976 May 4, *Bull. N.Z. Nat. Soc. Earthq. Eng.*, **11,** 191–192.

Ekstrom, G. & Engdahl, E. R., 1989. Earthquake source parameters and stress distribution in the Adak Island region of central Aleutian Islands, Alaska, *J. geophys. Res.* **94,** 15 499–15 519.

Fitch, T. J., 1972. Plate convergence, transcurrent faults, and internal deformation adjacent to southeast Asia and western Pacific, *J. geophys. Res.*, **77,** 4432–4460.

Forsyth, D. W., 1982. Determinations of focal depths of earthquakes associated with the bending of oceanic plates at trenches, *Phys. Earth planet. Inter.* **28,** 141–160.

Fredrich, J., McCaffrey, R. & Denham, D., 1988. Source parameters of seven large Australian earthquakes determined by body waveform inversion, *Geophys. J. Int.* **95,** 1–13.

Freund, R., 1971. The Hope Fault, a strike slip fault in New Zealand, *N.Z. Geol. Surv. Bull.* **86.**

Futterman, W. I., 1962. Dispersive body waves, *J. geophys. Res.*, **67,** 5279–5291.

Fukao, Y., 1973. Thrust faulting at a lithospheric plate boundary: the Portugal earthquake of 1969, *Earth planet. Sci. Lett.*, **18,** 205–216.

Gage, M., 1952. Greymouth coalfield, *N.Z. geol. Surv. Bull.*, **45.**

Grant, A. C., 1985. Structural evolution of the head of the Solander Trough, south of New Zealand, based on analysis of seismic basement, *N.Z. J. Geol. Geophys.*, **28,** 5–22.

Grimison, N. L., Chen, W.-P., 1986. The Azores–Gibraltar plate boundary: focal mechanisms, depths of earthquakes, and their tectonic implications, *J. geophys. Res.*, **91,** 2029–2047.

Grimison, N. L. & Chen, W.-P., 1988. Source mechanisms of four recent earthquakes along the Azores–Gibraltar plate boundary, *Geophys. J.* **92,** 391–401.

Haines, A. J., 1979. Seismic wave velocities in the uppermost mantle beneath New Zealand, *N.Z. J. Geol. Geophys.*, **22,** 245–257.

Haines, J., 1991a. 1968 Inangahua earthquake, (Abstract), *Neotectonics of the Buller Region Workshop*, Department of Scientific and Industrial Research Geology and Geophysics, New Zealand.

Haines, J., 1991b. 1929 Murchison earthquake, (Abstract), *Neotectonics of the Buller Region Workshop*, Department of Scientific and Industrial Research Geology and Geophysics, New Zealand.

Henderson, J., 1937. The west Nelson earthquakes of 1929, *N.Z. J. Sci. Technol.*, **19,** 66–143.

Houseman, G. & England, P., 1986. Finite strain calculations of continental deformation 1. Method and general results for convergent zones, *J. geophys. Res.* **91,** 3651–3663.

Isacks, B. & Molnar, P., 1969. Mantle earthquake mechanisms and the sinking of the lithosphere, *Nature*, **223,** 1121–1124.

Jackson, J., 1992. Partitioning of strike slip and convergent motion between Eurasia and Arabia in eastern Turkey and the Caucasus, *J. geophys. Res.*, **97,** 12 471–12 479.

Jackson, J. & Molnar, P., 1990. Active faulting and block rotations in the Western Transverse Ranges, California, *J. Geophys. Res.*, **95,** 22 073–22 087.

Jackson, J. A. & McKenzie, D. P., 1984. Active tectonics of the Alpine Himalayan belt between western Turkey and Pakistan, *Geophys. J. R. astr. Soc.*, **77,** 185–264.

Jarrard, R. D., 1986. Relations among subduction parameters, *Rev. Geophys.*, **24,** 217–284.

Johnson, T. & Molnar, P., 1972. Focal mechanisms and plate tectonics of the southwest Pacific. *J. geophys. Res.*, **77,** 5000–5032.

Jones, L. M., 1988. Focal mechanisms and the state of stress on the San Andreas Fault in southern California, *J. geophys. Res.*, **93,** 8869–8891.

Koons, P. O., 1989. The topographic evolution of collisional mountain belts: a numerical look at the Southern Alps, New Zealand, *Am. J. Sci.*, **289,** 1041–1069.

Koons, P. O., 1990. Two-sided orogen: collision and erosion from the sandbox to the Southern Alps, New Zealand, *Geology*, **18,** 679–682.

Lamb, S. H., 1988. Tectonic rotations about vertical axes during the last 4 Ma in part of the New Zealand plate-boundary zone, *J. struct. Geol.*, **10,** 875–893.

Lamb, S. H., 1989. Rotations about vertical axes in part of the New Zealand plate–boundary zone, theory and observations, in *Palaeomagnetic rotations and continental deformation,* pp. 473–488, eds Kissel, C. & Laj, C., Kluwer Academic Publishers, Dordrecht.

Lamb, S. H. & Bibby, H. M., 1989. The last 25Ma of rotational deformation in part of the New Zealand plate boundary zone, *J. struct. Geol.*, **11,** 473–492.

Lensen, G. J., 1970. Geological aspects of the Seddon earthquake, 1966, *Bull. New Zealand Dep. Sci. Indust. Res.*, **199,** 15–18.

Lensen, G. J., 1977. *Late Quaternary tectonic map of New Zealand,* 1:2,000,000 (1st edn.), New Zealand Geological Survey Miscellaneous Series, Map 12, Department of Scientific and Industrial Research, Wellington, New Zealand.

Lensen, G. J. & Suggate, R. P., 1968. Inangahua earthquake—preliminary account of the geology, in *Preliminary reports on the Inangahua earthquake, New Zealand, May 1968*, eds Adams, R. D., Eiby, G. A., Lowry, M. A., Lensen, G. J., Suggate, R. P. & Stephenson, W. R., *New Zealand Dept. Sci. Indust. Res. Bull.* **193,** 17–36.

McCaffrey, R., 1988. Active tectonics of the Eastern Sunda and Banda Arcs, *J. geophys. Res.*, **93,** 15 163–15 182.

McCaffrey, R., 1992. Oblique plate convergence, slip vectors, and forearc deformation, *J. geophys. Res.*, **97,** 8905–8915.

McCaffrey, R. & Abers, G., 1988. *SYN3: a program for inversion of teleseismic body waveforms on microcomputers,* Air Force Geophysics Laboratory Technical Report, AFGL-TR-88-0099, Air Force Geophysics Laboratory, Hanscom AFB, MA.

McCaffrey, R. & Nabelek, J., 1987. Earthquakes, gravity, and the origin of the Bali basin: an example of a nascent continental fold-and-thrust belt, *J. geophys. Res.*, **92,** 441–460.

McKenzie, D., 1969. The relation between fault plane solutions for earthquakes and the directions of principal stresses, *Bull. seism. Soc. Am.* **59,** 591–601.

Merzer, A. M. & Freund, R., 1974. Transcurrent faults, beam theory and the Marlborough Fault System, New Zealand, *Geophys. J. R. astr. Soc.*, **38,** 553–562.

Minster, J. B. & Jordan, T. H., 1978. Present-day plate motions, *J. geophys. Res.*, **83,** 5331–5354.

Molnar, P., 1979. Earthquake recurrence intervals and plate tectonics, *Bull. seism. Soc. Am.*, **69,** 115–133.

Molnar, P., 1990. *S*-wave residuals from earthquakes in the Tibetan region and lateral variations in the upper mantle, *Earth planet. Sci. Lett.*, **101,** 68–77.

Molnar, P. & Lyon-Caen, H., 1989. Fault-plane solutions of earthquakes and active tectonics of the Tibetan Plateau and its margins, *Geophys. J. Int.*, **99,** 123–153.

Molnar, P. & Tapponnier, P., 1975. Cenozoic tectonics of Asia: effects of a continental collision, *Science,* **189,** 419–426.

Mount, V. S. & Suppe, J., 1987. State of stress near the San Andreas fault: implications for wrench tectonics, *Geology,* **15,** 1143–1146.

Nabelek, J. L., 1984. Determination of earthquake source parameters from inversion of body waves, *PhD thesis,* MIT, MA.

Nathan, S., Anderson, H. J., Cook, R. A., Herzer, R. H., Hoskins, R. H., Raine, J. I. & Smale, D., 1986. *Cretaceous and Cenozoic sedimentary basins of the West Coast region, South Island, New Zealand,* New Zealand Geological Survey Basin Studies 1, Department of Scientific and Industrial Research, Wellington, New Zealand.

Nelson, M. R., McCaffrey, R. & Molnar, P., 1987. Source parameters for 11 earthquakes in the Tien Shan, Central Asia, determined by *P* and *SH* waveform inversion, *J. geophys. Res.*, **92,** 12 629–12 648.

Norris, R. J. & Carter, R. M., 1982. Fault-bounded blocks and their role in localising sedimentation and deformation adjacent to the Alpine Fault, southern New Zealand, *Tectonophysics,* **87,** 11–23.

Norris, R. J., Koons, P. O. & Cooper, A. F., 1990. The obliquely convergent plate boundary in the South Island of New Zealand: implications for ancient collision zones, *J. struct. Geol.*, **12,** 715–725.

Okal, E. A., 1992. On the orientation of the horizontal seismometers at South Pole, *Pure appl. Geophys.*, **138,** 151–154.

Reay, A., 1986. Andesites from Solander Island, *R. Soc. N.Z. Bull.*, **23,** 337–343.

Reyners, M., Gledhill, K. & Waters, D., 1991. Tearing of the subducted Australian plate during the Te Anau, New Zealand, earthquake of 1988 June 3, *Geophys. J. Int.*, **104,** 105–115.

Richardson, G. K., 1977. *Fowlers Fault site report,* New Zealand Geological Survey, Earth Deformation Section Report 43, New Zealand Department of Scientific and Industrial Research.

Robinson, R., 1986. Seismicity, structure and tectonics of the Wellington region, New Zealand, *Geophys. J. R. astr. Soc.*, **87,** 379–409.

Robinson, R., 1991. The Hawks Crag (Westport) earthquakes of January–February 1991, (Abstract), *Neotectonics of the Buller Region Workshop,* Department of Scientific and Industrial Research Geology and Geophysics, New Zealand.

Robinson, R., 1994. Shallow subduction and fault interaction: the Weber, New Zealand, earthquake sequence of 1991–1992, *J geophys. Res.*, in press.

Robinson, R. & Arabasz, W. J., 1975. Microearthquakes in the northwest Nelson region, New Zealand, *N.Z. J. Geol. Geophys.*, **18,** 83–91.

Ruff, L. J., Given, J. W., Sanders, C. O. & Sperber, C. M., 1989. Large earthquakes in the Macquarie Ridge complex: transitional tectonics and subduction initiation, *Pure appl. Geophys.*, **129,** 71–129.

Scholz, C. H. & Cowie, P. A., 1990. Determination of total strain from faulting using slip measurements, *Nature,* **346,** 837–839.

Scholz, C. H., Rynn, J. M. W., Weed, R. W. & Frohlich, C., 1973. Detailed seismicity of the Alpine Fault zone and Fiordland region, *Geol. Soc. Am. Bull.*, **84,** 3297–3316.

Smith, E. G. C. & Davey, F. J., 1984. Joint hypocentre determination of intermediate depth earthquakes in Fiordland, New Zealand, *Tectonophysics,* **104,** 127–144.

Smith, E. G. C. & Webb, T. H., 1986. The seismicity and related deformation of the Central Volcanic region, North Island, New Zealand, in Late Cenozoic Volcanism in New Zealand, ed. Smith, I. E. M., *R. Soc. N.Z. Bull.*, **23,** 112–133.

Souriac, A., 1984. Geoid anomalies over the Gorringe Ridge, North Atlantic Ocean, *Earth planet. Sci. Lett.*, **68,** 101–114.

Speight, R., 1933. The Arthur's Pass earthquake of 9th March, 1929, *N.Z. J. Sci. Technol.*, **15,** 173–182.

Stock, J. & Molnar, P., 1982. Uncertainties in the relative positions

of the Australia, Antarctica, Lord Howe, and Pacific plates since the late Cretaceous, *J. geophys. Res.*, **87,** 4697–4714.

Suggate, R. P., 1979. The Alpine Fault bends and the Marlborough faults, *R. Soc. N.Z. Bull.*, **18,** 16–72.

Taymaz, T., Jackson, J. & McKenzie, D., 1991. Active tectonics of the north and central Aegean Sea, *Geophys. J. Int.*, **106,** 433–490.

Taymaz, T., Jackson, J. & Westaway, R., 1990. Earthquake mechanisms in the Hellenic Trench near Crete, *Geophys. J. Int.*, **102,** 695–731.

van Dissen, R. & Yeats, R. S., 1991. Hope fault, Jordan thrust, and uplift of the Seaward Kaikoura Range, New Zealand, *Geology*, **19,** 393–396.

Walcott, R. I., 1978. Present tectonics and Late Cenozoic evolution of New Zealand, *Geophys. J. R. astr. Soc.*, **52,** 137–164.

Walcott, R. I., 1984. The kinematics of the plate boundary zone through New Zealand: a comparison of short- and long-term deformations, *Geophys. J. R. astr. Soc.*, **79,** 613–633

Ward, C. M., 1988. Marine terraces of the Waitutu district and their relation to the late Cenozoic tectonics of the southern Fiordland region, New Zealand, *J. R. Soc. N.Z.*, **18,** 1–28.

Webb, T. H., 1993. Spatial clustering and stress drops of foreshocks of the 1990 February Tennyson and Weber, New Zealand, earthquakes, *Bull. seism. Soc. Am.*, submitted.

Webb, T. H. & Kanamori, H., 1985. Earthquake focal mechanisms in the eastern Transverse Mountains, Southern California, and evidence for a regional decollement, *Bull. seism. Soc. Am.*, **75,** 737–757.

Webb, T. H. & Lowry, M. A., 1982. The Puysegur Bank earthquake of 1979 October 12, *N.Z. J. Geol. Geophys.*, **25,** 383–395.

Weins, D. A., 1987. Effects of near source bathymetry on teleseismic *P* waveforms, *Geophys. Res. Lett.*, **14,** 761–764.

Weins, D. A., 1989. Bathymetric effects on body waveforms from shallow subduction zone earthquakes and application to seismic processes in the Kurile Trench, *J. geophys. Res.*, **94,** 2955–2972.

Wellman, H. W., 1953. Data for the study of Recent and late Pleistocene faulting in the South Island of New Zealand, *N.Z. J. Sci. Technol.*, **B34,** 270–288.

Yang, J. S., 1991. The Kakapo Fault—a major active dextral fault in the central North Canterbury–Buller regions of New Zealand, *N.Z. J. Geol. Geophys.*, **34,** 137–143.

Yang, J. S., 1992. Landslide mapping and major earthquakes on the Kakapo Fault, South Island, New Zealand, *J. R. Soc. N.Z.*, **22,** 205–212.

Yeats, R. S., 1987. Tectonic map of Central Otago based on Landsat imagery, *N.Z. J. Geol. Geophys.*, **30,** 261–271.